iScience

CellPress
OPEN ACCESS

Article

ARMS-NF-κB signaling regulates intracellular ROS to induce autophagy-associated cell death upon oxidative stress

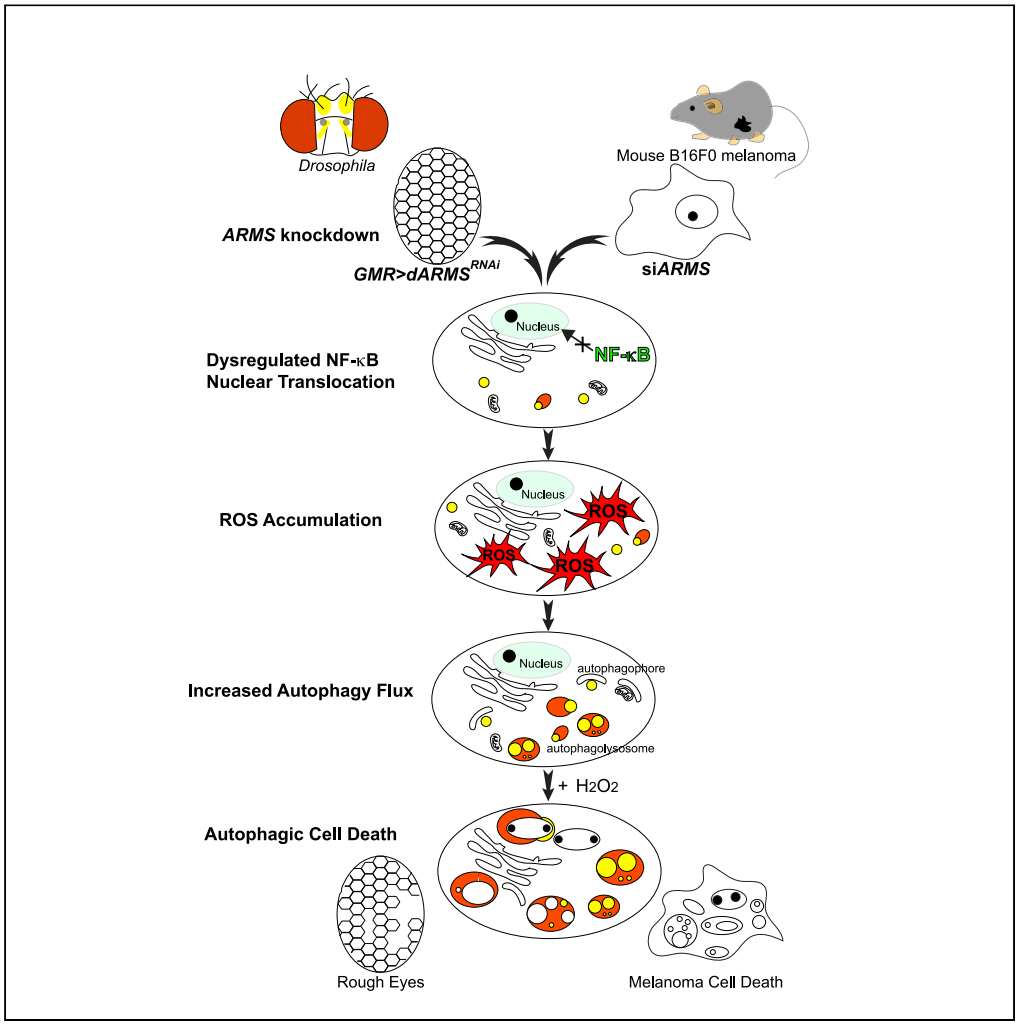

Yi-Hua Liao, June-Tai Wu, I-Chun Hsieh, Hsiu-Hsiang Lee, Pei-Hsin Huang

phhuang@ntu.edu.tw

Highlights

ARMS participates in the redox balance in neuronal and melanoma cells

Decreased ARMS compromises NF-κB nuclear translocation, leading to ROS accumulation

ROS accumulation caused by ARMS depletion augments autophagy flux

ROS-induced autophagy primed by ARMS reduction causes autophagic cell death on stress

Liao et al., iScience 26, 106005
February 17, 2023 © 2023 The Author(s).
https://doi.org/10.1016/j.isci.2023.106005

iScience

CellPress
OPEN ACCESS

Article

ARMS-NF-κB signaling regulates intracellular ROS to induce autophagy-associated cell death upon oxidative stress

Yi-Hua Liao,[1,3] June-Tai Wu,[1] I-Chun Hsieh,[3] Hsiu-Hsiang Lee,[2] and Pei-Hsin Huang[3,4,5,*]

SUMMARY

Ankyrin repeat-rich membrane spanning (ARMS) plays roles in neural development, neuropathies, and tumor formation. Such pleiotropic function of ARMS is often attributed to diverse ARMS-interacting molecules in different cell context. However, it might be achieved by ARMS' effect on global biological mediator like reactive oxygen species (ROS). We established *ARMS*-knockdown in melanoma cells (si*ARMS*) and in *Drosophila* eyes (*GMR>dARMS*^{RNAi}) and challenged them with H_2O_2. Decreased ARMS in both systems compromises nuclear translocation of NF-κB and induces ROS, which in turn augments autophagy flux and confers susceptibility to H_2O_2-triggered autophagic cell death. Resuming NF-κB activity or reducing ROS by antioxidants in si*ARMS* cells and *GMR>dARMS*^{RNAi} fly decreases intracellular peroxides level concurrent with reduced autophagy and attenuated cell death. Conversely, blocking NF-κB activity in wild-type flies/melanoma enhances ROS and induces autophagy with cell death. We thus uncover intracellular ROS modulated by ARMS-NFκB signaling primes autophagy for autophagic cell death upon oxidative stress.

INTRODUCTION

Ankyrin repeat-rich membrane spanning (ARMS), also known as Kidins220 (kinase D-interacting substrate of 220-kDa), is a transmembrane scaffold protein that has multiple biological functions through interacting with various molecules in different cellular contexts.[1–3] ARMS is involved in multiple aspects of neural development ranging from neuronal survival, axonal outgrowth, neuronal morphogenesis to synaptic plasticity.[4–9] Dysregulation of ARMS has been shown to correlate with several neuropathological changes. For example, genetic variant in *ARMS/KIDINS220* locus has been reported to be associated with increased risk of schizophrenia.[10] Downregulation of ARMS is observed in cerebral ischemia,[11] while enhanced ARMS expression is correlated with tauopathy in Alzheimer disease.[12]

ARMS is also involved in various kinds of tumor formation, which include cutaneous melanoma,[13,14] neuroblastoma,[15] and B cell acute lymphoblastic leukemia,[16] etc. We have previously shown that ARMS is overexpressed in more aggressive melanoma through activating MEK/ERK signaling to enable resistance to UVB-induced apoptosis.[13] Accordingly, reduced ARMS expression via RNAi in melanoma cells causes cells susceptible to apoptosis triggered by UVB. However, ARMS-knockdown resulted in cell death of melanoma cells challenged by hydrogen peroxide (H_2O_2) via a non-apoptotic process (Figures 1A–1C). We thus set out to investigate the mechanism underlying ARMS function upon cellular response to H_2O_2, which is one kind of reactive oxygen species (ROS).

ROS, including superoxide anion, hydroxyl radical, and H_2O_2, have long been regarded as destructive agents in various human diseases that include aging, cancers, and neurodegenerative diseases.[17,18] Nevertheless, under normal physiological and certain pathological conditions, ROS play a signaling rather than damaging role to modulate cell fate. Physiological level of ROS in the nervous system could regulate neurite growth, neuronal polarity establishment, and synaptic plasticity.[19] High-concentrated ROS generated from aberrant melanosomes in melanoma lead to cell senescence, autophagy, and cell death. On the contrary, long-term low-level oxidative stress in melanoma cells results in cell proliferation and contributes to drug resistance via activating nuclear factor-kappa B (NF-κB) and mitogen-activated protein kinase (MAPK) pathways.[20–23]

[1]Department of Dermatology, College of Medicine, National Taiwan University and National Taiwan University Hospital, Taipei 100, Taiwan

[2]Institute of Molecular Medicine, College of Medicine, National Taiwan University, Taipei 100, Taiwan

[3]Graduate Institute of Pathology, College of Medicine, National Taiwan University, Taipei 100, Taiwan

[4]Department of Pathology, National Taiwan University Hospital, Taipei 100, Taiwan

[5]Lead contact

*Correspondence: phhuang@ntu.edu.tw

https://doi.org/10.1016/j.isci.2023.106005

This is an open access article under the CC BY-NC-ND license (http://creativecommons.org/licenses/by-nc-nd/4.0/).

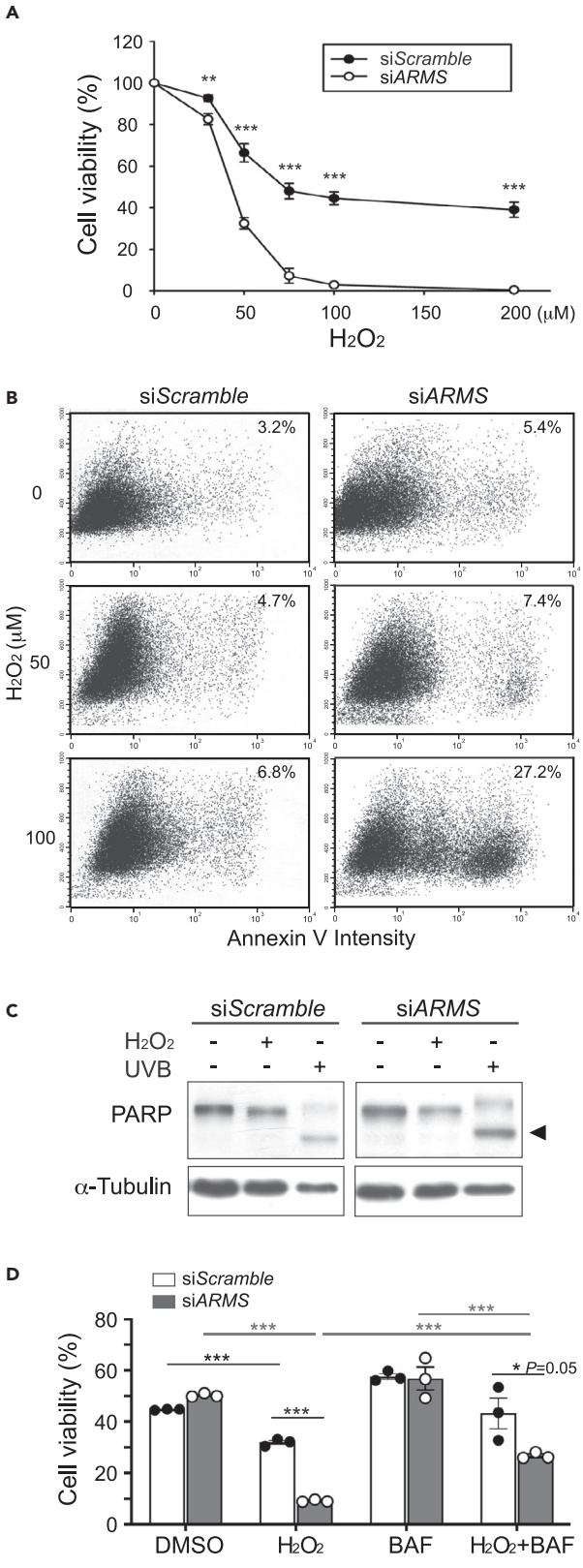
A
Cell viability (%)
siScramble
siARMS
H2O2
B
siScramble
siARMS
H2O2 (μM)
Annexin V Intensity
3.2%
5.4%
4.7%
7.4%
6.8%
27.2%
C
siScramble
siARMS
H2O2
UVB
PARP
α-Tubulin
D
siScramble
siARMS
Cell viability (%)
DMSO
H2O2
BAF
H2O2+BAF
* P=0.05

Figure 1. Non-apoptotic cell death induced by H_2O_2 in melanoma cells is augmented by *ARMS*-knockdown

(A) Dose-dependent effect of H_2O_2 on cell viability attenuated by ARMS silencing as revealed by MTT assay. The si*Scramble* and si*ARMS* B16-F0 melanoma cells were treated with the indicated concentration of H_2O_2 for 16 h. Data is represented as mean ± SD in triplicate experiments. **, $p < 0.01$; ***, $p < 0.001$, Student's *t* test.

(B) Apoptotic cell death assessed by flow cytometry with Annexin V staining of cells treated with 0, 50, or 100 μM H_2O_2, respectively, for 16 h.

(C) Western blot for PARP cleavage in cell lysates treated with UVB (25 mJ/cm^2) or 50 μM H_2O_2. Arrowhead, p85 cleaved form of PARP.

(D) Effect of pan-caspases inhibitor BAF on H_2O_2-induced cell death. Bar with dot graph shows mean ± SD in triplicate experiments, of which more than 200 cells were counted for each group. Cells were pretreated with 50 μM BAF for 30 min followed by 50 μM H_2O_2 for another 16 h. ***, $p < 0.001$, Student's *t* test.

Given that ARMS is functionally involved in neuropathology and tumor cells, of which the pathogenesis could be potentially modulated by ROS, we used *in vitro* melanoma cell line as a tumor model and *in vivo Drosophila* compound eye as a neurodegenerative model to investigate the causality of ROS in correlation with ARMS expression level. We report here that decreased ARMS expression in both melanoma cells and fly photoreceptors induces ROS through downregulating NF-κB activity. Such intracellular ROS accumulation primed by ARMS-knockdown augments autophagic flux, which in turn confers cells susceptible to autophagy-associated cell death challenged by oxidative stress.

RESULTS

ARMS-knockdown in melanoma cells promotes H_2O_2-induced cell death through a non-apoptotic process

H_2O_2 production in human melanoma cell culture has been demonstrated before[24] and is generated either as a byproduct during melanogenesis or develops after UV irradiation.[25] We thus used H_2O_2 as a physiology-mimicking stimulus for oxidative stress in this study. We have previously shown that knockdown of *ARMS* via siRNA in melanoma cells promoted cell death triggered by UVB and H_2O_2.[13] ARMS regulates UVB-induced cell demise via the mitochondrial apoptotic pathway,[13] but the way that ARMS modulates H_2O_2-induced death in melanoma is not known. MTT assay performed in mouse B16-F0 melanoma cell line showed a preferential cell-killing effect of H_2O_2 on *ARMS*-knockdown (si*ARMS*) cells over the si*Scramble* cells in a H_2O_2 concentration-dependent manner (Figure 1A). H_2O_2 at high concentration (≥100 μM) was deleterious to cells in part by activating apoptotic cell death, which was evidenced by that 27.2% of si*ARMS* cells were Annexin V-positive in comparison with 6.8% of si*Scramble* cells (Figure 1B). However, the increased cell-killing effect associated with ARMS knockdown at lower H_2O_2 concentration (50 μM) was apparently not mediated through apoptosis, given that neither increased Annexin V-positive cells nor PARP cleavage by activated Caspase 3 was detected (Figures 1B and 1C). Additionally, caspase inactivation by BAF treatment did not prevent si*ARMS* cells from H_2O_2-induced cell death at 50 μM H_2O_2 (Figure 1D). Together, it suggests a non-apoptotic cell death for preferential killing of *ARMS*-knockdown melanoma cells by low concentration of H_2O_2.

ARMS-knockdown in melanoma cells results in augmented autophagic flux with accumulation of autophagic vesicles

That H_2O_2 functions as an inducer for autophagy[26–28] leads us to examine whether autophagy was induced in si*ARMS* melanoma cells treated with 50 μM H_2O_2. Conversion of non-lipidated LC3-I to lipidated LC3-II (an indicator of active autophagy) was observed in both si*ARMS* and si*Scramble* cells without H_2O_2 treatment (Figure 2A), suggesting presence of active autophagy in melanoma cells at basal state. When treated with 50 μM H_2O_2, si*ARMS* cells showed increased expression of LC3-II compared with treated si*Scramble* cells (Figure 2A). Robust increase in the number and size of GFP-LC3 puncta was observed in si*ARMS* cells both at basal state and after H_2O_2 treatment (Figures 2B-a and 2B-c). By contrast, si*Scramble* cells showed diffuse cytoplasmic staining pattern with few scattered GFP-LC3 puncta (Figure 2B-a). *ARMS*-knockdown was causally related with the susceptibility for LC3-puncta accumulation in melanoma cells because re-introduction of RNAi-resistant ARMS resulted in reduction of GFP-LC3 puncta (Figures 2B-a and 2B-c). Furthermore, knockdown of ATG5 via lentiviral short hairpin RNA (shRNA) that led to 50% decrease in protein level (Figure 2B-b) caused significant decrease of GFP-LC3 puncta in si*ARMS* cells both at basal state and after H_2O_2 treatment (Figure 2B-a), suggesting that the GFP-LC3 puncta in si*ARMS* cells were formed via an ATG-dependent autophagy process. Transmission electron microscopy examination of si*ARMS* cells at basal state consistently showed presence of many autophagic vesicles characterized by double- or multiple-membrane autophagosomes sequestrating organelles (Figures 2C-a, upper panels, red

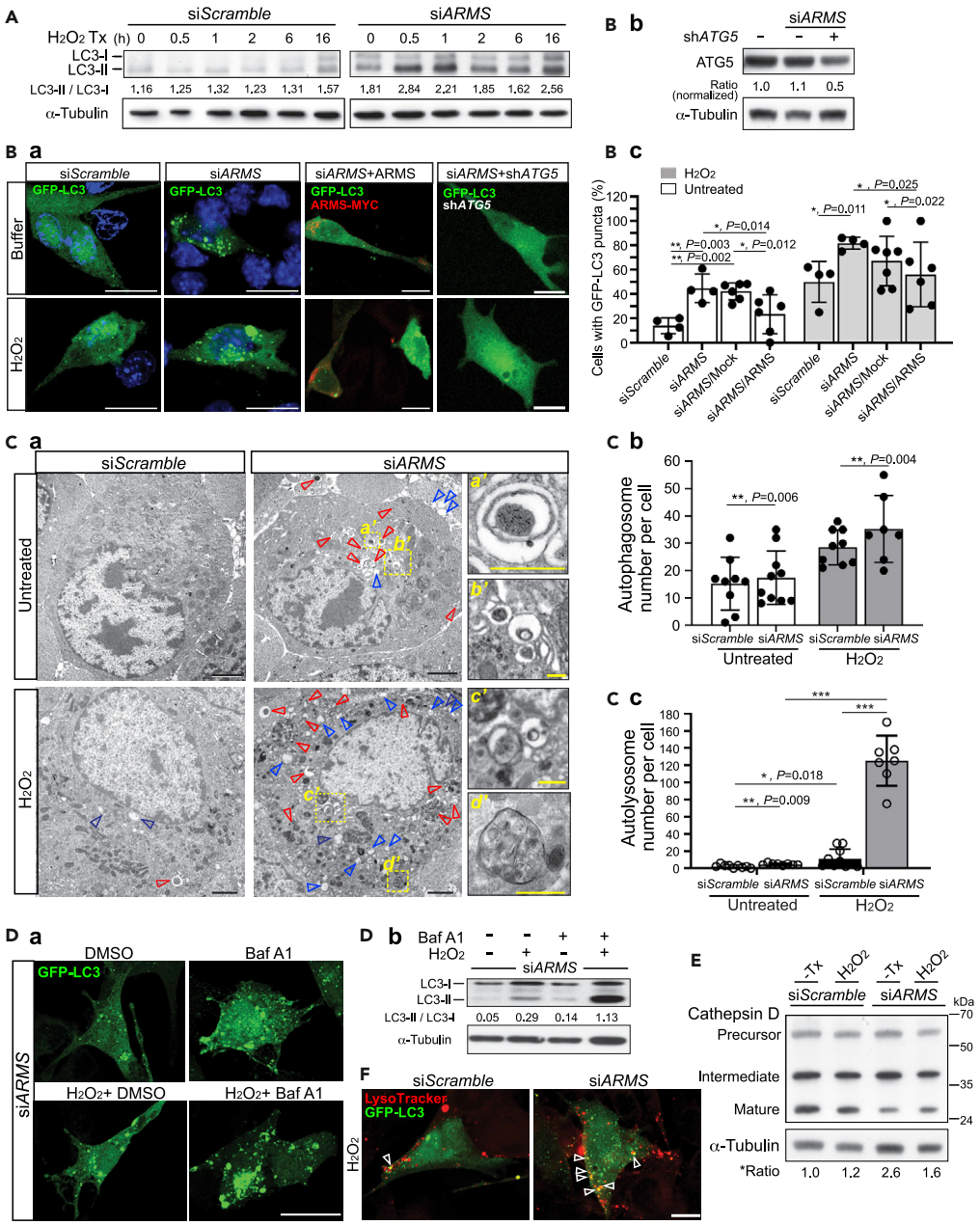

Figure 2. ARMS silencing leads to accumulation of autophagic vesicles and enhances H_2O_2-induced autophagy in melanoma cells

(A) Representative immunoblot and quantification of the relative LC3-II/LC3-I ratio during the time course of H_2O_2 treatment performed in si*Scramble* and si*ARMS* melanoma cells, respectively.

(B-a) Epifluorescence microscopy of H_2O_2-induced GFP-LC3 translocation (from diffuse cytoplasmic to granular punctate pattern) in GFP-LC3-transfected si*Scramble*, si*ARMS*, and si*ARMS* cells co-transfected with RNAi-resistant *ARMS*, or with sh*ATG5*, respectively. Scale bar, 20 μm.

(B-b) Western blot to show the efficacy of *ATG5*-knockdown in si*ARMS* cells infected by lentiviral-sh*ATG5* and treated with 50 μM H_2O_2 for 16 h.

(B-c) Bar graph (mean ± SD) combined with dot plot to show the percentage of cells having GFP-LC3 translocation in si*ARMS* cells compared with si*Scramble* cells at baseline and after 16-h treatment of H_2O_2. The value of each dot was derived from the counting of 100–110 cells. *, $p < 0.05$; **, $p < 0.01$, Mann-Whitney rank-sum test.

(C-a) Transmission electron microscopy of the si*Scramble* and si*ARMS* cells before and after treatment with 50 μM H_2O_2 for 16 h. The autophagic vacuoles seen in si*ARMS* cells (dashed insets in a', b') were magnified. Red empty arrowheads,

Figure 2. *Continued*

double-membrane or multi-membrane autophagosomes; Blue empty arrowheads, single-membrane autolysosomes with residual digested material. Black scale bar, 2 μm; Yellow scale bar, 500 nm. Quantification analysis of autophagosomes (C-b) and autolysosomes (C-c) derived from transmission electron microscopy in si*ARMS* cells compared with si*Scramble* cells at baseline and after 16-h treatment of H_2O_2. **, $p < 0.01$; ***, $p < 0.001$, Mann-Whitney rank-sum test.

(D) Effect of Bafilomycin A1 (Baf A1) treatment on the level of autophagosome formation in si*ARMS* cells as revealed by immunofluorescence study of intracellular GFP-LC3 dots (D-a) and immunoblotting of LC3-II (D-b). The cells were pretreated with 10 nM Baf A1 or buffer 1 h before H_2O_2 treatment. Scale bar, 20 μm. See also Figure S1A.

(E) Representative Western blotting of the processed forms of Cathepsin D in si*Scramble* and si*ARMS* cells with or without H_2O_2 treatment. *, the ratio of intermediate (46 kDa) plus precursor form (54 kDa) to mature form (32 kDa) of Cathepsin D.

(F) Co-localization and fusion (yellow fluorescence indicated by white empty arrowheads) of GFP-LC3-positive autophagic vesicles with the lysosomes (labeled by LysoTracker red) in H_2O_2-treated si*ARMS* cells. Scale bar, 10 μm.

arrowheads) and single-membrane autolysosomes containing residual digested materials or empty vacuoles (Figure 2C-a, blue arrowheads; boxed regions magnified in Figures 2C-a-a′ and 2C-a-b′). Dramatic increase in the number of autophagic vacuoles was seen in si*ARMS* cells treated with 50 μM H_2O_2 for 16 h (Figure 2C-a, lower panels. higher magnification of boxed regions in Figure 2C-a-c′, 2C-a-d′; quantification analysis shown in Figures 2C-b and 2C-c). By contrast, just few autophagosomes and autolysosomes were observed in H_2O_2-treated si*Scramble* cells (Figures 2C-a, -b and -c). These data collectively suggest that decreased ARMS expression in melanoma cells results in accumulation of autophagic vesicles both at basal state and in response to H_2O_2.

Autophagy is a dynamic process, starting with the *de novo* formation of double-membrane vesicles and undergoes a stepwise process involving membrane elongation, maturation, and fusion with endosomes/lysosomes for degradation of engulfed cytosolic materials/organelles.[29,30] Accordingly, the accumulation of autophagic vesicles in si*ARMS* cells could either result from upregulation of autophagosome formation or from an impaired autophagic maturation/degradation process. To address this issue, we examined autophagic flux by measuring LC3-II level in the presence of bafilomycin A1 (Baf A1), an inhibitor of autophagosome fusion/degradation.[31,32] Baf A1 treatment in si*ARMS* cells further increased the number of GFP-LC3 puncta (Figures 2D-a and S1A) and the level of LC3-II (Figure 2D-b) both at basal state and after H_2O_2 treatment, suggesting that upregulated autophagosome formation rather than defective autophagosome degradation is related to the accumulation of autophagic vacuoles via ARMS depletion. In line, the protein level of ATG5 and Beclin-1, both regulating autophagosome biogenesis, was slightly increased in si*ARMS* cells (Figures 2B and S1B). A higher ratio of pro-Cathepsin D (52 or 46 kDa) to mature Cathepsin D (32 kDa), which is used as a measurement of autophagy activity because extensive vacuolization during active autophagy impairs vesicular trafficking of pro-Cathepsin D from the ER into the lysosomes for maturation,[33,34] was also observed in si*ARMS* cells (Figure 2E).

Augmented autophagy flux with increased autophagy vesicles observed in si*ARMS* cells further suggests that lysosomal protein degradation capacity might be enhanced with ARMS-knockdown. Indeed, the protein level of p62/SQSTM1, a substrate for lysosomal protease,[35] was decreased in si*ARMS* cells (Figure S1C). Given that autophagic vacuoles acquire protein degradation capacity via becoming acidified and obtaining lysosomal enzymes through serial fusion events with late endosomes and lysosomes, we analyzed the status of acidic compartments in si*ARMS* cells by a vital lysotropic dye-acridine orange, which emits bright red fluorescence while accumulated in acidic organelles.[36] As shown in Figure S1D, an increase in red fluorescence intensity upon H_2O_2 treatment was exclusively seen in si*ARMS* cells, suggesting an enhancement of acidified vesicular organelles in H_2O_2-treated *ARMS*-knockdown cells. Additionally, co-localization of GFP-LC3-rimmed vesicles with acidic compartment stained by the live acidophilic dye LysoTracker Red was also observed in H_2O_2-treated si*ARMS* cells (Figure 2F, white empty arrowhead), even though some fused vesicles could be unnoticed due to fluorescently quenched GFP-LC3 in acidified compartments. Altogether, decreased ARMS expression in melanoma cells results in increased autophagic flux that leads to accumulation of autophagic vesicles with enhanced autophagy activity.

Enhanced autophagy in si*ARMS* melanoma leads to H_2O_2-induced cell death

Autophagy in cancer cells performs either cytoprotective or cytotoxic function depending on cell context.[37] Electronic microscopy of H_2O_2-treated si*ARMS* cells showed that most of the nuclei appeared intact

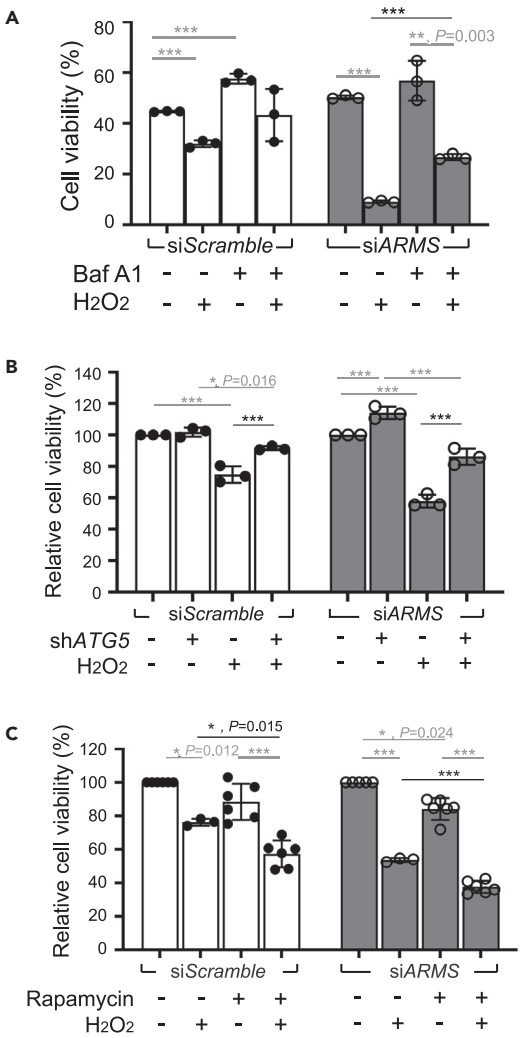

Figure 3. H_2O_2-induced cell death in melanoma cells is associated with autophagy

Effect of autophagy inhibition by bafilomycin A1 (Baf A1, 10 nM) (A) or by *ATG5*-knockdown (B), or of enhanced autophagy by pretreatment with rapamycin (50 nM) (C) on cell survival of si*Scramble* and si*ARMS* cells treated with H_2O_2. Bar graphs show mean ± SD in at least three independent MTT assays (P.S. The exact experimental number is indicated by dots). The values in (B) and (C) were normalized with those derived from untreated cells of the same genomic background (The viability of untreated cells was set as 100% for each genotype as the reference point.). *, $p < 0.05$; **, $p < 0.01$; ***, $p < 0.001$, Welch's *t*-test for (A), Kruskal-Wallis one-way analysis of variants on ranks for (B), and One-way ANOVA with Hokm-Sidak test for (C).

without chromatin condensation or nuclear fragmentation (Figure 2C-a), which was in line with few Annexin V-positive apoptotic cells detected by flow cytometry (Figure 1B). We then investigated whether augmented autophagy in si*ARMS* cells contributes to autophagic cell death triggered by H_2O_2. If active autophagy in si*ARMS* cells was unfavorable for survival under oxidative stress, inhibition of autophagy would attenuate cell death. Otherwise, accelerated cell death would be observed by inhibition of autophagy if autophagy was cytoprotective. When autophagy was blocked by Baf A1, H_2O_2-induced cell death in *ARMS*-knockdown cells was significantly suppressed (Figure 3A). Inhibition of autophagosome formation by ATG5 knockdown increased baseline cell viability and attenuated H_2O_2-induced cell death of si*ARMS* cells (Figure 3B). Conversely, promotion of autophagy by pretreatment with rapamycin, an inhibitor of mTOR that negatively regulates autophagy, accentuated H_2O_2-induced cell death (Figure 3C). These data suggest that active autophagy related to decreased ARMS expression in melanoma cells is causally linked to oxidative stress-induced cell death.

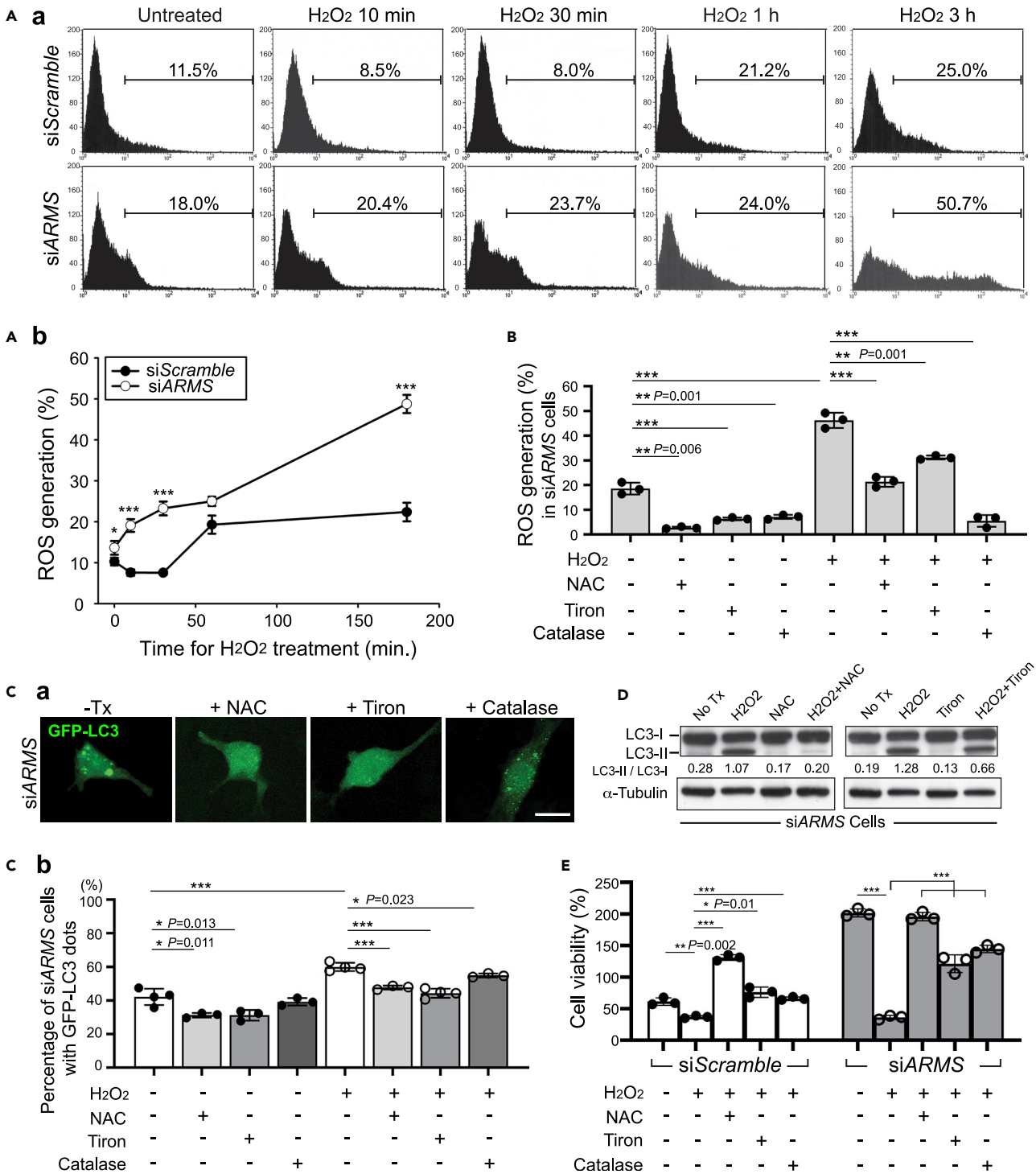

Figure 4. ARMS-knockdown primes ROS accumulation to induce autophagy and autophagic cell death triggered by H_2O_2

(A) ARMS-knockdown results in intracellular ROS accumulation. Intracellular ROS was determined by flow cytometry with CM-H_2DCFDA staining at baseline and after H_2O_2 treatment for 10 min, 30 min, 1 h, and 3 h, respectively. ROS accumulation along the time course of H_2O_2 is shown representatively in histogram (A-a) and in the diagram (A-b) showing mean ± SD in triplicate experiments. *, $p < 0.05$; ***, $p < 0.001$, Student's *t* test.

(B) Addition of antioxidants N-acetyl cysteine (NAC, 1 μM), tiron (2 μM), or PEG-catalase (1000 IU) for 1 h attenuated intracellular ROS formation in si*ARMS* cells. **, $p < 0.01$; ***, $p < 0.001$, Student's *t* test. See also Figure S1E.

Figure 4. *Continued*

(C) Representative confocal microscopy (C-a) and quantification (C-b) of GFP-LC3 dots in si*ARMS* cells pretreated with NAC, tiron, or PEG-catalase. Bar with dot graph shows mean ± SD in triplicate experiments. *, $p < 0.05$; ***, $p < 0.001$, One Way ANOVA with Holm-Sidak method. Scale bar, 20 μm.

(D) Immunoblot and quantification of the relative LC3-II/LC3-I ratio in lysates derived from H_2O_2-treated si*ARMS* cells pre-incubated with NAC or tiron.

(E) Cell viability assessed by MTT assay in si*Scramble* and si*ARMS* cells pretreated with antioxidants (NAC, tiron, or PEG-catalase, respectively). Bar with dot graph shows mean ± SD in triplicate experiments. *, $p < 0.05$; ***, $p < 0.001$, One Way ANOVA with Holm-Sidak method.

Decreased expression of ARMS primes intracellular ROS accumulation to induce autophagy

We speculated that decreased expression of ARMS might participate in the establishment of cellular stress, which in turn induces autophagy. Given that H_2O_2 treatment resulted in more autophagic vesicles in si*ARMS* cells and that ROS served as one of the signaling molecules for autophagy induction,[38] we measured the intracellular oxidants by using the cell-permeable fluorescent probe 2′, 7′-dichlorodihydro-fluorescein diacetate, which reacted specifically with peroxide and emitted fluorescence on 488 nm excitation. Flow cytometry showed an increased level of intracellular peroxide in si*ARMS* cells at basal state compared with that of the si*Scramble* cells (Figures 4A-a and 4A-b). When challenged with H_2O_2, si*ARMS* cells accumulated much higher amount of intracellular peroxide than si*Scramble* cells at the indicated time up to 5 h post H_2O_2 treatment (Figures 4A-a and 4A-b). Pretreatment of antioxidants including the thiol-reducing agent N-acetyl cysteine (a glutathione precursor), tiron (a vitamin E analog), or polyethylene glycol-catalase (a H_2O_2-degrading enzyme) efficiently reduced the intracellular ROS level in si*ARMS* cells both at basal state and after H_2O_2 treatment (Figures 4B and S1E). Pretreatment of the ROS scavengers also attenuated H_2O_2-induced translocation of GFP-LC3 (Figures 4C-a and 4C-b), decreased the conversion of LC3-II from LC3-I (Figure 4D), and blocked H_2O_2-induced cell death (Figure 4E) in si*ARMS* cells. The data collectively suggest that ARMS reduction in melanoma cells establishes higher level of intracellular ROS at baseline and mounts a more prominent accumulation of intracellular ROS triggered by H_2O_2. Besides, the enhanced ROS accumulation primed by decreased ARMS in melanoma cells leads to augmented autophagy, which is associated with increased cell death triggered by oxidative stress.

Knockdown of *dARMS* in *Drosophila* eye leads to retinal degeneration in adult fly with concomitant accumulation of autophagic vesicles, which are causally linked to intracellular ROS

To evaluate the contribution of ARMS to autophagy *in vivo*, we turned to the fruit fly by selectively knocking down *Drosophila ARMS* (*dARMS*/CG42672) in specific subsets of cells using the *GAL4/UAS* (*upstream activating sequence*) system. Because ARMS was abundantly expressed in neural tissues and was functionally involved in neuron growth, differentiation, and death,[1,2] we selectively knocked down dARMS in photoreceptor cells by expressing *dARMS-dsRNA* under the control of the pan-retinal *glass multiple reporter* (*GMR*)-*GAL4* driver.[39] Two fly lines of *dARMS*-knockdown were established using *dARMS-dsRNA* corresponding to two different, non-overlapped sequences of *dARMS* gene (designated as $GMR>dARMS^{RNAi\#1}$ and $GMR>dARMS^{RNAi\#2}$, respectively; see STAR Methods, experimental model and subject details), and the rough eye phenotype caused by photoreceptor neuron degeneration was assessed and scored.[40] Semi-quantitative RT-PCR analysis of mRNA derived from the fly eyes expressing either *dARMS-dsRNA* showed decreased expression of *dARMS* transcript (≥50% decrease) with slightly enhanced knockdown of *dARMS* in those expressing *dARMS-dsRNA#2* (Figure 5A). We first examined whether there was any defect in the development of the visual system at the larva stage. No obvious morphological difference was seen in the eye discs, optic stalks, and optic lobes of the $GMR>dARMS^{RNAi}$ larva shown by *UAS-mCD8::GFP* driven by *GMR-GAL4* (Figures S2A and S2B). GFP-labeled presynaptic proteins (GFP fused with presynaptic vesicle protein Synaptotagmin (Syt:GFP) or Synaptobrevin (Syb:GFP)) were detected in the distal tips of photoreceptor axons with similar intensity between wild-type and *dARMS*-knockdown larva, suggesting normal protein transportation from cell body to the distal axons of retinal neurons in $GMR>dARMS^{RNAi}$ larva (Figure S2C). In spite of normal developmental processes of the eyes, adult flies with *dARMS* knockdown exhibited a rough eye phenotype characterized by ommatidial pitting, disorganization, fusion, and abnormal/supernumerary inter-ommatidial bristles (Figures 5B-a and 5B-b).The severity of eye phenotype was dependent on the expression level of dARMS, with higher severity score seen in fly eyes expressing *dARMS-dsRNA#2* than those with *dARMS-dsRNA#1*, and Dicer-overexpressing flies ($GMR>dARMS^{RNAi\#1}$,*Dicer*) showing even severer phenotype (Figures 5B-a and 5B-b). The eye defect seen in $GMR>dARMS^{RNAi}$ fly was specifically attributed to *dARMS* knockdown because overexpressing dARMS in fly eyes ($GMR>dARMS^{RNAi}$, *dARMS*) attenuated rough eye phenotype (Figure 5B). Ultrastructural examination of fly eyes by transmission electron microscopy showed that flies with *dARMS* knockdown contained many vesicles featuring autophagosomes or autophagolysosomes in the cytoplasm of the

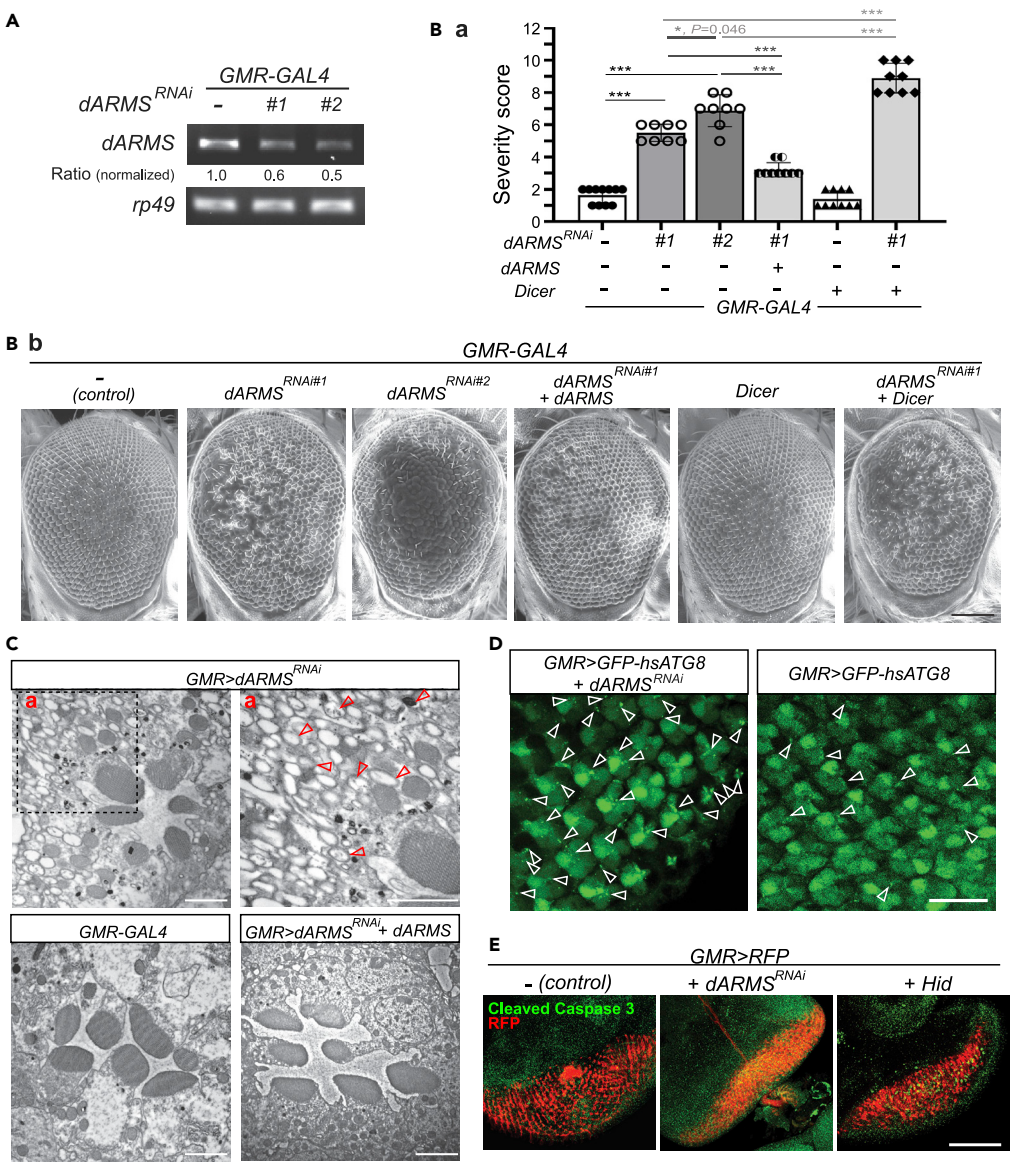

Figure 5. *dARMS*-knockdown in *Drosophila* eyes causes retinal degeneration associated with robust autophagy in adult fly

(A) Effective RNAi of dARMS by *ARMS-dsRNA* shown by semi-quantitative RT-PCR analysis of *dARMS* transcript extracted from adult *Drosophila* compound eyes. Rp49 was used as an internal loading control.

(B-a) Representative scanning electron microscopy (SEM) images of 1-day-old fly eyes of the indicated genotypes reared at 27°C. Scale bar, 100 μm. (B-b) Quantitative analyses of the rough eye phenotype by objective scoring of the SEM images (Pandey et al., 2007). Data are presented as mean ± SD *, $p < 0.05$; ***, $p < 0.001$, One-way ANOVA with Duncan's method.

(C) Representative transmission electron micrographs of *GMR>dARMS*^{RNAi} fly eyes, in comparison with the control wild-type *GMR-GAL4* and with the *GMR>dARMS*^{RNAi}, *dARMS* flies. Higher magnification of the dashed inset (C-a) demonstrated the double-membrane autophagic vesicles (red empty arrowheads) in *GMR>dARMS*^{RNAi} fly eyes. Scale bar, 2 μm. See also Figure S2D.

(D) Distribution of GFP-hsATG8-positive dots (white empty arrowheads) in eye imaginal discs from the third-instar larvae by confocal microscopy. Scale bar, 25 μm.

(E) Representative fluorescence micrographs of eye imaginal discs from the third-instar larvae labeled by transgenic RFP (*GMR>RFP*) and co-stained with antibodies against cleaved Caspase 3. Scale bar, 100 μm.

photoreceptors (Figures 5C-a and S2D). Overexpression of dARMS in the *dARMS*-knockdown flies (*GMR>dARMS*^{RNAi}, *dARMS*) reduced the level of autophagic vesicles to that of the *GMR-GAL4* flies (Figure 5C). GFP-conjugated *Homo sapiens* ATG8 (GFP-hsATG8) also highlighted much more numbers of autophagic vesicles (GFP + dots) in the photoreceptors of *GMR>dARMS*^{RNAi} fly (Figure 5D, empty white arrowheads). By contrast, the *GMR-GAL4* flies showed diffuse cytoplasmic expression of GFP with some concentrated intensity in the rhabdomeres (Figure 5D). The eye imaginal discs of *GMR>dARMS*^{RNAi} larva and of the *GMR-GAL4* control showed similar diffuse cytosolic pattern of immunolabeled cleaved Caspase 3, which on cleavage would display focal cytosolic discrete dot patterns as seen in the eye discs of *GMR>RFP,Hid* larva that underwent constitutive neuronal apoptosis[41] (Figure 5E). Therefore, *GMR>dARMS*^{RNAi} flies did not reveal apoptosis in retinal neurons. Combined, it suggests that reduced expression of dARMS in *Drosophila* eyes causes photoreceptor degeneration with concurrent accumulation of autophagic vesicles.

To investigate whether ROS observed in si*ARMS* melanoma cells also occurred in the photoreceptors of the fly with *dARMS* knockdown, we stained the eye imaginal discs of the wandering third-instar larvae with CM-H_2DCFDA to detect peroxides. As expected, the number of CM-H_2DCFDA-positive cells with eye-expressing red fluorescent protein was markedly increased in *GMR>RFP, dARMS*^{RNAi} fly eyes compared with the control *GMR>RFP* fly (Figure 6A). Decreasing ROS by overexpressing the ROS scavenger Catalase in *dARMS*-depleted fly eyes (*GMR>dARMS*^{RNAi}, *Catalase*), as evidenced by reduced CM-H_2DCFDA-stained dots (Figure 6A), suppressed the severity of rough eye phenotype (Figure 6B) and concomitantly reduced the numbers of autophagic vacuoles (Figure 6C). Conversely, application of H_2O_2 over the fly eyes with *dARMS*-knockdown accentuated rough eye phenotype (Figure 6D). These data collectively suggest a causal effect of oxidative stress-induced autophagy and neurodegeneration in adult fly eyes harboring low level of dARMS.

Compromised NF-κB activity underlies intracellular ROS accumulation and autophagy induction in *ARMS*-knockdown cells

Neurotrophin-induced nuclear factor-κB (NF-κB) activation is involved in melanoma cell survival under cell stress[42–44] and in neuronal survival through activated MAPK and IKK signaling, which is downstream of TRK-interacting ARMS.[45] Besides, NF-κB activity could modulate intracellular ROS level by regulating its target genes including *SOD1*, *SOD2*, and *Catalase* that encode proteins involved in redox reaction and balance. Conversely, ROS could function as a trigger of NF-κB activity.[46–48] We thus examined whether *ARMS*-knockdown causes intracellular ROS accumulation and autophagic cell death through NF-κB signaling. The NF-κB-driven luciferase reporter was transfected into si*ARMS* cells to show a significant reduction in the basal and H_2O_2-induced NF-κB transcriptional activity compared to si*Scramble* cells (Figure 7A). Nuclear translocation of RelA, a subunit of NF-κB responsible for NF-κB transcriptional activity, was also attenuated in si*ARMS* cells compared with si*Scramble* cells after 2-h treatment of H_2O_2 (Figures 7B and S3A). RelA phosphorylation, which mediates its nuclear localization,[49] was decreased in si*ARMS* cells both at basal and under H_2O_2-treated conditions comopared with that in si*Scramble* cells (Figure S3B). We thus conclude that low expression level of ARMS in melanoma cells is closely associated with decreased NF-κB activity that might be caused by compromised nuclear translocation of NF-κB.

The causal relationship between si*ARMS*-mediated ROS and NF-κB activity was further investigated. Intracellular peroxide assessed in si*ARMS* cells transfected with wild-type IKKβ to resume the NF-κB activity showed reduced ROS level, which was further attenuated in constitutively active IKKβ (IKKβ-SS/EE)-transfected si*ARMS* cells (Figures 7C, S3C, and S3D). By contrast, overexpressing constitutively inactivated IKKβ (IKKβ-SS/AA) in si*ARMS* cells did not attenuate intracellular ROS (Figures 7C and S3D). To correlate NF-κB activity with si*ARMS*-mediated autophagy, GFP-LC3 dots were quantified to reveal that overexpressing wild-type IKKβ and constitutively active IKKβ-SS/EE in si*ARMS* cells inhibited LC3 translocation, whereas expression of constitutively inactivated IKKβ-SS/AA did not (Figure 7D). Conversely, blocking NF-κB signaling in si*Scramble* cells by Bay 11–7082, an irreversible inhibitor of IκBα phosphorylation,[50] enhanced LC3 translocation to a level comparable to that in si*ARMS* cells at basal state and after H_2O_2 treatment (Figure 7E). The data collectively suggest that compromised NF-κB activity in *ARMS*-knockdown cells functions upstream of intracellular ROS accumulation and autophagy activity.

To corroborate the above findings *in vivo*, we decreased NF-κB activity in *GMR>dARMS*^{RNAi} fly eyes by knocking down the *Drosophila* NF-κB gene homolog *dorsal* (*dL*). *GMR>dARMS*^{RNAi}, *dl*^{dsRNA} flies tended

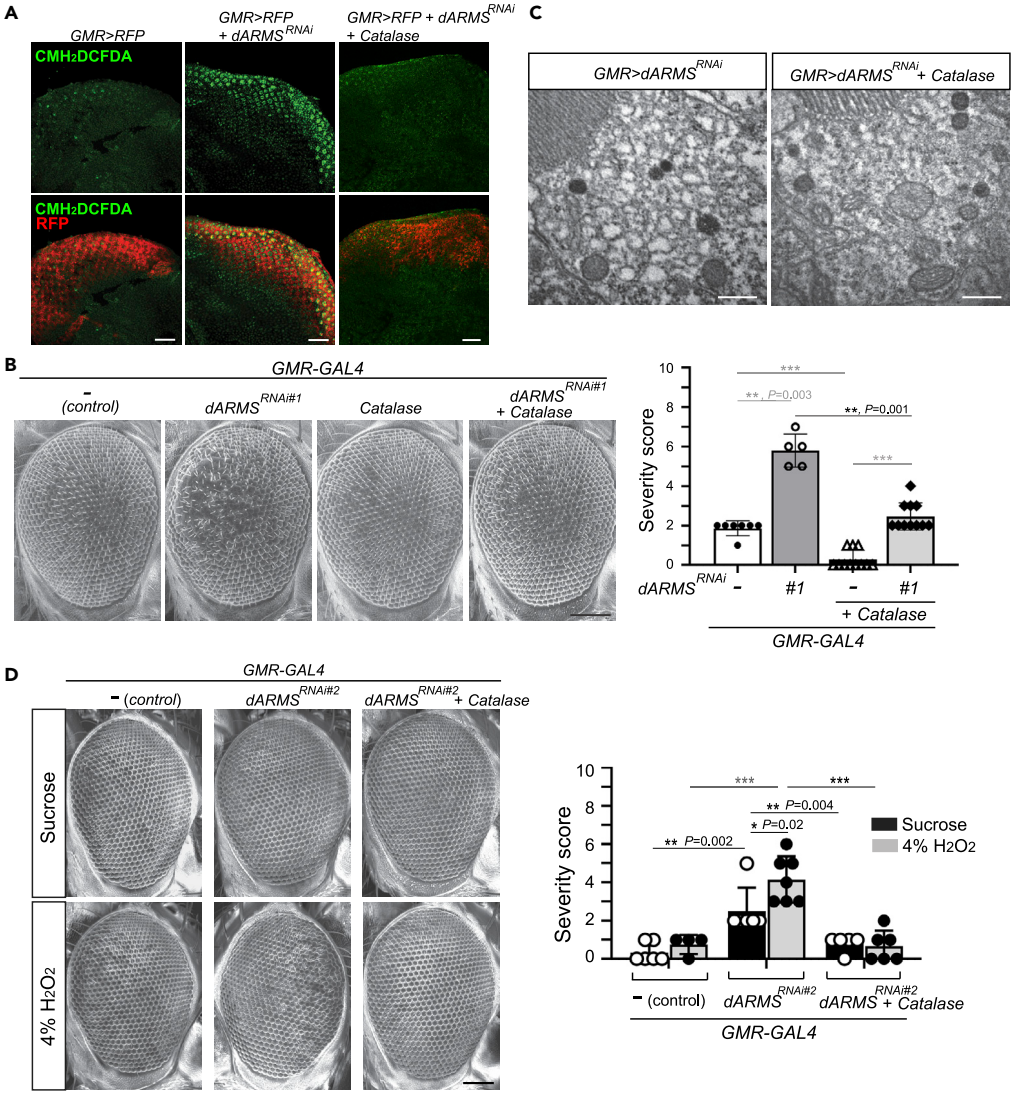

Figure 6. Increased ROS causally associates with autophagic death of photoreceptor cells in *GMR>dARMS^{RNAi}* adult flies

(A) Representative fluorescence micrographs of ROS production (labeled by green fluorescent dye CM-H_2DCFDA) in the eye imaginal discs (labeled by transgenic RFP fluorescence) from the third-instar larvae. Scale bar, 50 μm.

(B) SEM images of 1-day-old fly eyes of the indicated genotypes reared at 27°C. Scale bar, 100 μm. Quantitative analysis of the rough eye phenotype by objective scoring of the SEM images of the indicated genotype. Data are shown as mean ± SD; **, $p < 0.01$; ***, $p < 0.001$, Mann-Whitney rank-sum test.

(C) Transmission electron microscopy to show that overexpression of Catalase in *dARMS^{RNAi}* flies (*GMR>dARMS^{RNAi}, Catalase*) decreased autophagic vacuoles caused by *dARMS*-knockdown. Scale bar, 500 nm.

(D) 1-day-old flies were kept in vials with filter paper soaked with 4% H_2O_2 dissolved in 5% sucrose solution or in 5% sucrose solution alone (without H_2O_2) for 48 h. Representative scanning electron microscope images of fly eyes (**Left**) and the scoring of rough eye phenotype (**Right**) showed increased severity of rough eyes in H_2O_2-treated flies with *dARMS*-knockdown (*GMR>dARMS^{RNAi}*), which could be partially rescued by overexpressing Catalase (*GMR>dARMS^{RNAi}, Catalse*). Scale bar, 100 μm *, $p < 0.05$; **, $p < 0.01$; ***, $p < 0.001$; Mann-Whitney rank-sum test.

to have severer rough eye phenotype than that caused by knocking down *dARMS* alone (Figure 7F). Conversely, increasing NF-κB activity by crossing with the IKKβ gain-of-function allele *IKKβ^{EY02434}* with *GMR>dARMS^{RNAi}* fly (*GMR>dARMS^{RNAi},IKKβ^{EY02434}*) attenuated the severity of the rough eye caused by *dARMS*-knockdown (Figure 7F). An inverse correlation between the amount of autophagy vacuoles and the level of NF-κB activity in *GMR>dARMS^{RNAi}* fly was further demonstrated by transmission electron

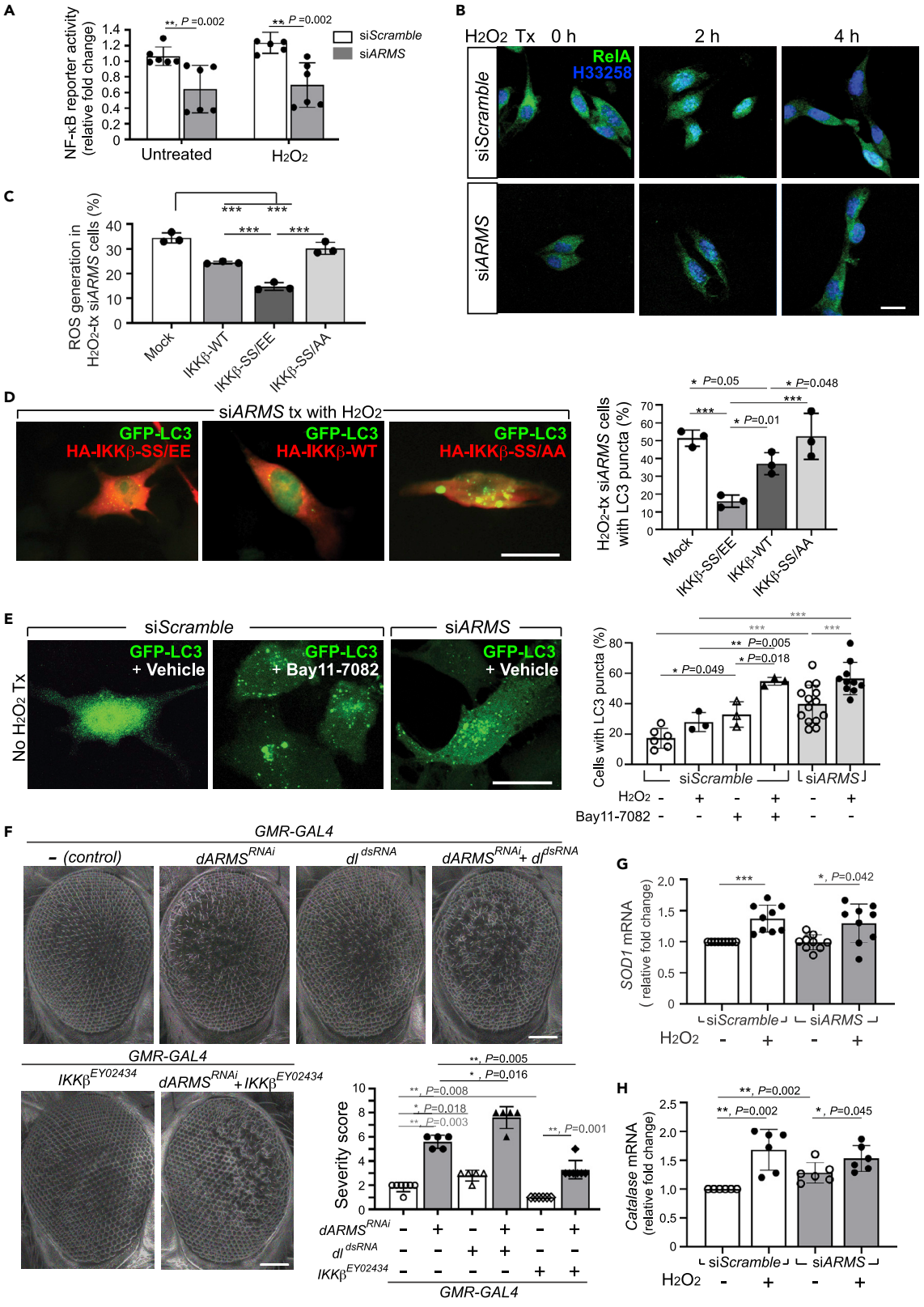
A
NF-κB reporter activity (relative fold change)
**, P =0.002
** P =0.002
siScramble
siARMS
Untreated
H2O2
B
H2O2 Tx 0 h
2 h
4 h
RelA
H33258
siScramble
siARMS
C
ROS generation in H2O2-tx siARMS cells (%)
***
Mock
IKKβ-WT
IKKβ-SS/EE
IKKβ-SS/AA
D
siARMS tx with H2O2
GFP-LC3
HA-IKKβ-SS/EE
HA-IKKβ-WT
HA-IKKβ-SS/AA
H2O2-tx siARMS cells with LC3 puncta (%)
* P=0.05
* P=0.048
* P=0.01
E
siScramble
siARMS
No H2O2 Tx
GFP-LC3
+ Vehicle
+ Bay11-7082
Cells with LC3 puncta (%)
** P=0.005
* P=0.018
* P=0.049
H2O2
Bay11-7082
F
GMR-GAL4
- (control)
dARMSRNAi
dldsRNA
dARMSRNAi+ dldsRNA
IKKβEY02434
dARMSRNAi+IKKβEY02434
Severity score
**, P=0.005
* , P=0.016
** P=0.008
* P=0.018
** P=0.003
**, P=0.001
G
SOD1 mRNA (relative fold change)
***
*, P=0.042
H
Catalase mRNA (relative fold change)
**, P=0.002
**, P=0.002
*, P=0.045

Figure 7. Compromised NF-κB activation resulting from *ARMS*-knockdown underlies intracellular ROS and ROS-induced autophagy

(A) Basal and H_2O_2-stimulated transcriptional activity of NF-κB in si*ARMS* cells compared with the si*Scramble*. Cells were co-transfected with the NF-κB luciferase reporter and the CMV-β-gal plasmids. 48 h post-transfection, the cells were left untreated or treated with H_2O_2 for another 2 h. Relative luciferase activities were calculated based on β-gal values in each transfection. The value for luciferase activity in untreated si*Scramble* cells was designated as 1.

(B) Fluorescence microscopy to show nuclear translocation of RelA in si*Scramble* but not in si*ARMS* cells 2 h after H_2O_2 treatment. Scale bar, 20 μm.

(C) Bar graph shows intracellular ROS determined by flow cytometry with CM-H_2DCFDA staining in H_2O_2-treated si*ARMS* cells co-transfected with HA-tagged mock vector, wild-type IKKβ (IKKβ-WT), constitutively active IKKβ (IKKβ-SS/EE), or constitutively inactive IKKβ (IKKβ-SS/AA), respectively.

(D) Representative fluorescence microscopy images (left panels) and quantification analysis to show GFP-LC3 translocation in H_2O_2-treated si*ARMS* cells co-transfected with the indicated plasmid. Scale bar, 20 μm.

(E) Confocal microscopy and quantification analysis of GFP-LC3 puncta showed that inactivation of NF-κB by Bay 11–7082 in si*Scramble* cells increased basal and H_2O_2-induced autophagy to the level comparable with si*ARMS* cells. Scale bar, 20 μm.

(F) SEM images of 1-day-old fly eyes of the indicated genotypes reared at 27°C with scores of the rough eye phenotype. Scale bar, 100 μm.

(G and H) Quantitative RT-PCR analyses of *SOD1* (G) and *Catalase* (H) transcripts in H_2O_2-treated si*ARMS* cells compared with si*Scramble cells*. Data information: all values are shown as mean ± SD *, $p < 0.05$; **, $p < 0.01$; ***, $p < 0.001$; *p* values on the basis of Mann-Whitney rank-sum test (A, F, G, and H), or of One Way ANOVA with Duncan's multiple range test (C, D, and E).

microscopy. More autophagosomes and autophagolysosomes were observed in the eyes of *GMR>dARMS*^{RNAi}, *dI*^{dsRNA} fly, whereas much less amount of autophagic vacuoles were seen in the eyes of *GMR>dARMS*^{RNAi},*IKKβ*^{EY02434} fly (Figure S3E). Accordingly, in line with what was observed in si*ARMS* melanoma cells, attenuating NF-κB activity in *Drosophila* eyes with *dARMS*-knockdown enhances photoreceptor degeneration accompanied with more autophagic vacuoles, while augmenting NF-κB activity rescues the rough eye phenotype caused by *dARMS*-knockdown with concomitant decreased autophagy.

The transcriptional target genes regulated by NF-κB include antioxidant enzymes *Catalase* and *SOD1*.[46,47] We speculate that low NF-κB activity in si*ARMS* cells might transcriptionally silence antioxidants so that imbalanced redox by lower amounts of antioxidants leads to ROS accumulation. Indeed, real-time PCR analysis showed reduced induction of *SOD1* and *Catalase* mRNA in si*ARMS* cells upon H_2O_2 treatment compared with si*Scramble* cells (Figures 7G and 7H). Immunoblot also showed relatively decreased expression of Catalase and SOD1 in H_2O_2-treated si*ARMS* cells (Figures S3F and S3G). We also checked the expression level and the activity of Nrf2 (nuclear factor E2-related factor 2), another critical transcriptional factor for upregulation of antioxidant genes via the p62/Keap1/Nrf2 signal pathway functioning mainly in non-neuronal cells.[19,51] As shown in Figures S3H–S3J, the expression level of Nrf2 protein was similar between si*ARMS* cells and si*Scramble* cells at basal state and was similarly slightly increased in both cell lines after H_2O_2 treatment (Figure S3H). To evaluate Nrf2 signaling activity, the transcript expression level of two Nrf2 target genes *Nqo1* (NADPH quinone dehydrogenase 1) and *Txnrd1* (Thioredoxin reductase 1) was examined.[52] Both si*ARMS* and si*Scramble* cells had similar mRNA expression level of *Nqo1* and *Txnrd1* at basal state (Figures S3I and S3J). Upon H_2O_2 challenge, increased expression of *Nqo1* and *Txnrd1* mRNA was similarly observed in both cell lines, with even a little bit higher amount of *Nqo1* mRNA in H_2O_2-treated si*ARMS* cells (Figures S3I and S3J). Thus, Nrf2 signaling for transcriptional regulation of the antioxidant system is not compromised in si*ARMS* cells so that intracellular ROS accumulation in si*ARMS* cells could not be attributed to dysregulated Nrf2 signaling. We conclude that decreased ARMS expression causes attenuated NF-κB activity so that antioxidants could not be properly upregulated in response to oxidative stress. Accumulation of intracellular ROS follows to induce autophagy, which in turn promotes autophagic cell death challenged by oxidative stress.

DISCUSSION

How ARMS plays its role in diverse pathological processes remains an interesting issue based on its potential therapeutic manipulation in multiple diseases. Although multiple ARMS-interacting molecules in different cellular context are proposed to underscore ARMS' pleiotropic function, our study provides another possibility that intracellular ROS modulated by the expression level of ARMS could underlie ARMS' broad involvement in neuropathology and cancers. Intracellular ROS accumulation in cells with *ARMS*-knockdown is likely to be mediated via two different ways: decreased transcription of ROS scavengers by downregulating NF-κB activity and enhanced degradation of ROS scavenger proteins through augmented autophagy flux. By this way, *ARMS*-knockdown render cells into a vicious cycle to accumulate more ROS, causing cells vulnerable to oxidant-induced autophagic cell death.

That ROS contributes to autophagy-dependent cell death has been well documented in plants, cancers, and neurodegenerative diseases.[53–55] In line, we demonstrate intracellular ROS accumulation attributed

to lower expression of ARMS induces autophagy and autophagic cell death both in fly eyes to present retinal degeneration and in malignant melanoma. Our study thus raises a concern about the exploitation of autophagy inhibitors in treating melanoma. Based on the notion that autophagy is cytoprotective, inhibition of autophagy in melanoma has been shown to prevent cancer cells from survival and to attenuate cancer growth and aggressiveness.[56,57] However, for aggressive melanoma that often overexpresses ARMS[13,14] and is highly chemoresistant due to its anti-apoptotic effect,[58] we suggest manipulation upon decreasing ARMS expression level combined with autophagy enhancers, rather than autophagy inhibitors, to activate ROS-induced autophagic cell death for effective treatment.

Although autophagy is causally related to neuron degeneration, autophagy is dispensable for embryonic neurogenesis and neural stem cell maintenance. It is only beyond postnatal stage that neurodegenerative phenotype caused by disrupted autophagy becomes obvious.[59–61] For example, loss of ATG proteins causes no gross structural changes in developing mouse brains despite highly active autophagy in early neurodevelopmental stage.[62] Radial glial cell-specific deletion of FIP200, which is one component of the ULK1-Atg13-FIP200-Atg101 complex essential for autophagy induction, causes no abnormality of the developing cortex.[63] Here, we reveal that *ARMS*-knockdown in *Drosophila* photoreceptor cells has little effect on the development of fly compound eyes but is apt to autophagy-associated retinal degeneration at adult age.

Autophagy participates not only in neuronal death but also in neuronal differentiation. Inhibition of autophagy results in an increased dendritic spine density of postnatal neurons, indicating the requirement of autophagy for dendritic pruning.[64–66] Noticeably, $ARMS^{+/-}$ mice revealed decreased dendritic complexity in the pyramidal neurons of barrel cortex and in the granule cells of the dentate gyrus only in adults, but not in embryos and adolescents.[5] We thus speculate that such neuronal phenotype in adult $ARMS^{+/-}$ mice might in part result from augmented autophagy caused by lower level of ARMS expression (30%–40% decrease of ARMS protein shown in Wu's paper[5]). In conclusion, we uncover that ARMS participates in the regulation of intracellular ROS that could trigger autophagy. Given that ARMS is ubiquitously expressed in neurons that often show pathogenic aberrant accumulation of autophagic vacuoles in postmortem brains of various neurodegenerative diseases,[67,68] it merits further investigation of ARMS' role and ROS-induced autophagy in different human neurodegenerative disorders.

Limitations of the study

Several limitations of our study should be noted. First, because ARMS has diverse interaction with many different proteins in distinct cellular contexts, our finding that ARMS-NF-κB-ROS signal axis determines cell demise in melanoma and in retinal degeneration may not be applicable to other cancer types or other neurodegenerative diseases. Second, although our analyses on *Drosophila* genetics were controlled for genotypes and age, the sample size of our study is relatively small. However, our results closely mirror the findings from melanoma cells. We are thus confident that our results in this relatively small sample are generalizable. Third, the causal relationship among ARMS protein level, MAPK signaling, and NF-κB activity was not explored in this study. The complexity of crosstalk among ROS, MAPK, NF-κB, and other signaling pathways was not investigated here, too. It should be noted that ROS is often caused by increased MAPK to augment NF-κB activity,[69] and enhanced NF-κB could downregulate ROS and MAPK activity via a negative feedback loop.[70] However, there is no validation that decreased MAPK would necessarily downregulate intracellular ROS. Although our previous study shows that decreased expression of ARMS in melanoma cells leads to attenuated MAPK signaling,[13] it is not proper to infer that reduced MAPK activity in si*ARMS* cells would not cause ROS accumulation. The paradox remains to be solved by further dissecting the nature of the relationship among multiple stress-related signal pathways in cells with ARMS-knockdown.

STAR★METHODS

Detailed methods are provided in the online version of this paper and include the following:

- KEY RESOURCES TABLE
- RESOURCE AVAILABILITY
  - Lead contact
  - Materials availability
  - Data and code availability

SUPPLEMENTAL INFORMATION

Supplemental information can be found online at https://doi.org/10.1016/j.isci.2023.106005.

ACKNOWLEDGMENTS

We thank Ms. Hsin-Lin Yang for technique help. This work was supported by the Ministry of Science and Technology, the Republic of China (MOST103-2314-B-002-067-MY3; 106-2314-B-002-116-MY3) granted to Y.-H.L., by National Taiwan University Hospital (NTUH98P26-2) and "Center of Precision Medicine" from the featured area research center program within the framework of the Higher Education Sprout Project by the Ministry of Education (No. NTU-108L9014) granted to P.-H.H.

AUTHOR CONTRIBUTIONS

Study design: Y.-H.L., J.-T.W., P.-H.H.; Obtaining funding: Y.-H.L., P.-H.H.; Conducting experiments: Y.-H.L., I.-C.H.; Analyzing data: Y.-H.L., J.-T.W., H.-H.L., I.-C.H., P.-H.H.; Drafting the manuscript: Y.-H.L.; Critical Reviewing and Revision of the manuscript: P.-H.H. with the help of H.-H.L. on *Drosophila* genetics. All authors agree to be responsible for the work for ensuring that questions related to the integrity and accuracy of any part of the work are appropriately investigated and resolved.

DECLARATION OF INTERESTS

We report no potential conflict of interest.

Received: August 14, 2022
Revised: November 23, 2022
Accepted: January 13, 2023
Published: February 17, 2023

REFERENCES

1. Iglesias, T., Cabrera-Poch, N., Mitchell, M.P., Naven, T.J., Rozengurt, E., and Schiavo, G. (2000). Identification and cloning of Kidins220, a novel neuronal substrate of protein kinase D. J. Biol. Chem. *275*, 40048–40056. https://doi.org/10.1074/jbc.M005261200.

2. Kong, H., Boulter, J., Weber, J.L., Lai, C., and Chao, M.V. (2001). An evolutionarily conserved transmembrane protein that is a novel downstream target of neurotrophin and ephrin receptors. J. Neurosci. *21*, 176–185. https://doi.org/10.1523/jneurosci.21-01-00176.2001.

3. Raza, M.Z., Allegrini, S., Dumontet, C., and Jordheim, L.P. (2018). Functions of the multi-interacting protein KIDINS220/ARMS in cancer and other pathologies. Genes Chromosomes Cancer *57*, 114–122. https://doi.org/10.1002/gcc.22514.

4. Arévalo, J.C., Yano, H., Teng, K.K., and Chao, M.V. (2004). A unique pathway for sustained neurotrophin signaling through an ankyrin-rich membrane-spanning protein. EMBO J. *23*, 2358–2368. https://doi.org/10.1038/sj.emboj.76002535.

5. Wu, S.H., Arévalo, J.C., Sarti, F., Tessarollo, L., Gan, W.B., and Chao, M.V. (2009). Ankyrin Repeat-rich Membrane Spanning/Kidins220 protein regulates dendritic branching and spine stability in vivo. Dev. Neurobiol. *69*, 547–557. https://doi.org/10.1002/dneu.20723.

6. Arévalo, J.C., Wu, S.H., Takahashi, T., Zhang, H., Yu, T., Yano, H., Milner, T.A., Tessarollo, L., Ninan, I., Arancio, O., and Chao, M.V. (2010). The ARMS/Kidins220 scaffold protein modulates synaptic transmission. Mol. Cell. Neurosci. *45*, 92–100. https://doi.org/10.1016/j.mcn.2010.06.002.

7. Higuero, A.M., Sánchez-Ruiloba, L., Doglio, L.E., Portillo, F., Abad-Rodríguez, J., Dotti, C.G., and Iglesias, T. (2010). Kidins220/ARMS modulates the activity of microtubule-regulating proteins and controls neuronal polarity and development. J. Biol. Chem. *285*, 1343–1357. https://doi.org/10.1074/jbc.M109.024703.

8. Duffy, A.M., Schaner, M.J., Wu, S.H., Staniszewski, A., Kumar, A., Arévalo, J.C., Arancio, O., Chao, M.V., and Scharfman, H.E. (2011). A selective role for ARMS/Kidins220 scaffold protein in spatial memory and trophic support of entorhinal and frontal cortical neurons. Exp. Neurol. *229*, 409–420. https://doi.org/10.1016/j.expneurol.2011.03.008.

9. Chen, Y., Fu, W.Y., Ip, J.P.K., Ye, T., Fu, A.K.Y., Chao, M.V., and Ip, N.Y. (2012). Ankyrin repeat-rich membrane spanning protein

(kidins220) is required for neurotrophin and ephrin receptor-dependent dendrite development. J. Neurosci. *32*, 8263–8269. https://doi.org/10.1523/jneurosci.1264-12.2012.

10. Kranz, T.M., Goetz, R.R., Walsh-Messinger, J., Goetz, D., Antonius, D., Dolgalev, I., Heguy, A., Seandel, M., Malaspina, D., and Chao, M.V. (2015). Rare variants in the neurotrophin signaling pathway implicated in schizophrenia risk. Schizophr. Res. *168*, 421–428. https://doi.org/10.1016/j.schres.2015.07.002.

11. López-Menéndez, C., Gascón, S., Sobrado, M., Vidaurre, O.G., Higuero, A.M., Rodríguez-Peña, A., Iglesias, T., and Díaz-Guerra, M. (2009). Kidins220/ARMS downregulation by excitotoxic activation of NMDARs reveals its involvement in neuronal survival and death pathways. J. Cell Sci. *122*, 3554–3565. https://doi.org/10.1242/jcs.056473.

12. López-Menéndez, C., Gamir-Morralla, A., Jurado-Arjona, J., Higuero, A.M., Campanero, M.R., Ferrer, I., Hernández, F., Ávila, J., Díaz-Guerra, M., and Iglesias, T. (2013). Kidins220 accumulates with tau in human Alzheimer's disease and related models: modulation of its calpain-processing by GSK3β/PP1 imbalance. Hum. Mol. Genet. *22*, 466–482. https://doi.org/10.1093/hmg/dds446.

13. Liao, Y.H., Hsu, S.M., and Huang, P.H. (2007). ARMS depletion facilitates UV irradiation induced apoptotic cell death in melanoma. Cancer Res. *67*, 11547–11556. https://doi.org/10.1158/0008-5472.Can-07-193014.

14. Liao, Y.H., Hsu, S.M., Yang, H.L., Tsai, M.S., and Huang, P.H. (2011). Upregulated ankyrin repeat-rich membrane spanning protein contributes to tumour progression in cutaneous melanoma. Br. J. Cancer *104*, 982–988. https://doi.org/10.1038/bjc.2011.1815.

15. Jung, H., Shin, J.H., Park, Y.S., and Chang, M.S. (2014). Ankyrin repeat-rich membrane spanning (ARMS)/Kidins220 scaffold protein regulates neuroblastoma cell proliferation through p21. Mol. Cell *37*, 881–887. https://doi.org/10.14348/molcells.2014.0182.

16. Sakamoto, K., Imamura, T., Kanayama, T., Yano, M., Asai, D., Deguchi, T., Hashii, Y., Tanizawa, A., Ohshima, Y., Kiyokawa, N., et al. (2017). Ph-like acute lymphoblastic leukemia with a novel PAX5-KIDINS220 fusion transcript. Genes Chromosomes Cancer *56*, 278–284. https://doi.org/10.1002/gcc.22433.

17. Gilgun-Sherki, Y., Melamed, E., and Offen, D. (2001). Oxidative stress induced-neurodegenerative diseases: the need for antioxidants that penetrate the blood brain barrier. Neuropharmacology *40*, 959–975. https://doi.org/10.1016/s0028-3908(01)00019-318.

18. Uttara, B., Singh, A.V., Zamboni, P., and Mahajan, R.T. (2009). Oxidative stress and neurodegenerative diseases: a review of upstream and downstream antioxidant therapeutic options. Curr. Neuropharmacol. *7*, 65–74. https://doi.org/10.2174/157015909787602823.

19. Oswald, M.C.W., Garnham, N., Sweeney, S.T., and Landgraf, M. (2018). Regulation of neuronal development and function by ROS. FEBS Lett. *592*, 679–691. https://doi.org/10.1002/1873-3468.12972.

20. Fruehauf, J.P., and Trapp, V. (2008). Reactive oxygen species: an Achilles' heel of melanoma? Expert Rev. Anticancer Ther. *8*, 1751–1757. https://doi.org/10.1586/14737140.8.11.1751.

21. Trachootham, D., Lu, W., Ogasawara, M.A., Nilsa, R.D.V., and Huang, P. (2008). Redox regulation of cell survival. Antioxidants Redox Signal. *10*, 1343–1374. https://doi.org/10.1089/ars.2007.1957.

22. Lee, J., Giordano, S., and Zhang, J. (2012). Autophagy, mitochondria and oxidative stress: cross-talk and redox signalling. Biochem. J. *441*, 523–540. https://doi.org/10.1042/bj20111451.

23. Gidanian, S., Mentelle, M., Meyskens, F.L., Jr., and Farmer, P.J. (2008). Melanosomal damage in normal human melanocytes induced by UVB and metal uptake–a basis for the pro-oxidant state of melanoma. Photochem. Photobiol. *84*, 556–564. https://doi.org/10.1111/j.1751-1097.2008.00309.x24.

24. Bittinger, F., González-García, J.L., Klein, C.L., Brochhausen, C., Offner, F., and Kirkpatrick, C.J. (1998). Production of superoxide by human malignant melanoma cells. Melanoma Res. *8*, 381–387. https://doi.org/10.1097/00008390-199810000-00001.

25. Nappi, A.J., and Vass, E. (1996). Hydrogen peroxide generation associated with the oxidations of the eumelanin precursors 5,6-dihydroxyindole and 5,6-dihydroxyindole-2-carboxylic acid. Melanoma Res. *6*, 341–349. https://doi.org/10.1097/00008390-199610000-00001.

26. Scherz-Shouval, R., and Elazar, Z. (2007). ROS, mitochondria and the regulation of autophagy. Trends Cell Biol. *17*, 422–427. https://doi.org/10.1016/j.tcb.2007.07.009.

27. Chen, Y., McMillan-Ward, E., Kong, J., Israels, S.J., and Gibson, S.B. (2008). Oxidative stress induces autophagic cell death independent of apoptosis in transformed and cancer cells. Cell Death Differ. *15*, 171–182. https://doi.org/10.1038/sj.cdd.440223328.

28. Filomeni, G., De Zio, D., and Cecconi, F. (2015). Oxidative stress and autophagy: the clash between damage and metabolic needs. Cell Death Differ. *22*, 377–388. https://doi.org/10.1038/cdd.2014.15029.

29. Nakatogawa, H., Suzuki, K., Kamada, Y., and Ohsumi, Y. (2009). Dynamics and diversity in autophagy mechanisms: lessons from yeast. Nat. Rev. Mol. Cell Biol. *10*, 458–467. https://doi.org/10.1038/nrm2708.

30. Yu, L., Chen, Y., and Tooze, S.A. (2018). Autophagy pathway: cellular and molecular mechanisms. Autophagy *14*, 207–215. https://doi.org/10.1080/15548627.2017.1378838.

31. Klionsky, D.J., Abdelmohsen, K., Abe, A., Abedin, M.J., Abeliovich, H., Acevedo Arozena, A., Adachi, H., Adams, C.M., Adams, P.D., Adeli, K., et al. (2016). Guidelines for the use and interpretation of assays for monitoring autophagy. Autophagy *12*, 1–222. https://doi.org/10.1080/15548627.2015.1100356.

32. Mizushima, N., and Yoshimori, T. (2007). How to interpret LC3 immunoblotting. Autophagy *3*, 542–545. https://doi.org/10.4161/auto.460033.

33. Zeng, X., Overmeyer, J.H., and Maltese, W.A. (2006). Functional specificity of the mammalian Beclin-Vps34 PI 3-kinase complex in macroautophagy versus endocytosis and lysosomal enzyme trafficking. J. Cell Sci. *119*, 259–270. https://doi.org/10.1242/jcs.0273534.

34. Klionsky, D.J. (2009). Autophagy in mammalian systems, Part B. Preface. Methods Enzymol. *452*. xxi-xxii. https://doi.org/10.1016/s0076-6879(08)03631-8.

35. Larsen, K.B., Lamark, T., Øvervatn, A., Harneshaug, I., Johansen, T., and Bjørkøy, G. (2010). A reporter cell system to monitor autophagy based on p62/SQSTM1. Autophagy *6*, 784–793. https://doi.org/10.4161/auto.6.6.12510.

36. Glick, D., Barth, S., and Macleod, K.F. (2010). Autophagy: cellular and molecular mechanisms. J. Pathol. *221*, 3–12. https://doi.org/10.1002/path.2697.

37. Fulda, S. (2017). Autophagy in cancer therapy. Front. Oncol. *7*, 128. https://doi.org/10.3389/fonc.2017.00128.

38. Azad, M.B., Chen, Y., and Gibson, S.B. (2009). Regulation of autophagy by reactive oxygen species (ROS): implications for cancer progression and treatment. Antioxidants Redox Signal. *11*, 777–790. https://doi.org/10.1089/ars.2008.2270.

39. Freeman, M. (1996). Reiterative use of the EGF receptor triggers differentiation of all cell types in the Drosophila. Cell *87*, 651–660. https://doi.org/10.1016/S0092-8674(00)81385-940.

40. Pandey, U.B., Nie, Z., Batlevi, Y., McCray, B.A., Ritson, G.P., Nedelsky, N.B., Schwartz, S.L., DiProspero, N.A., Knight, M.A., Schuldiner, O., et al. (2007). HDAC6 rescues neurodegeneration and provides an essential link between autophagy and the UPS. Nature *447*, 859–863. https://doi.org/10.1038/nature05853.

41. Song, Z., Guan, B., Bergman, A., Nicholson, D.W., Thornberry, N.A., Peterson, E.P., and Steller, H. (2000). Biochemical and genetic interactions between Drosophila caspases and the proapoptotic genes rpr, hid, and grim. Mol. Cell Biol. *20*, 2907–2914. https://doi.org/10.1128/mcb.20.8.2907-2914.2000.

42. Ramirez, S.H., Sanchez, J.F., Dimitri, C.A., Gelbard, H.A., Dewhurst, S., and Maggirwar, S.B. (2001). Neurotrophins prevent HIV Tat-induced neuronal apoptosis via a nuclear factor-kappaB (NF-kappaB)-dependent mechanism. J. Neurochem. *78*, 874–889. https://doi.org/10.1046/j.1471-4159.2001.00467.x.

43. Mattson, M.P., and Meffert, M.K. (2006). Roles for NF-kappaB in nerve cell survival, plasticity, and disease. Cell Death Differ. *13*, 852–860. https://doi.org/10.1038/sj.cdd.440183744.

44. Madonna, G., Ullman, C.D., Gentilcore, G., Palmieri, G., and Ascierto, P.A. (2012). NF-κB as potential target in the treatment of melanoma. J. Transl. Med. *10*, 53. https://doi.org/10.1186/1479-5876-10-5345.

45. Sniderhan, L.F., Stout, A., Lu, Y., Chao, M.V., and Maggirwar, S.B. (2008). Ankyrin-rich membrane spanning protein plays a critical role in nuclear factor-kappa B signaling. Mol. Cell. Neurosci. *38*, 404–416. https://doi.org/10.1016/j.mcn.2008.04.001.

46. Zhou, L.Z., Johnson, A.P., and Rando, T.A. (2001). NF kappaB and AP-1 mediate transcriptional responses to oxidative stress in skeletal muscle cells. Free Radic. Biol. Med. *31*, 1405–1416. https://doi.org/10.1016/s0891-5849(01)00719-547.

47. Rojo, A.I., Salinas, M., Martín, D., Perona, R., and Cuadrado, A. (2004). Regulation of Cu/Zn-superoxide dismutase expression via the phosphatidylinositol 3 kinase/Akt pathway and nuclear factor-kappaB. J. Neurosci. *24*, 7324–7334. https://doi.org/10.1523/jneurosci.2111-04.200448.

48. Morgan, M.J., and Liu, Z.G. (2011). Crosstalk of reactive oxygen species and NF-κB signaling. Cell Res. *21*, 103–115. https://doi.org/10.1038/cr.2010.17849.

49. Hoffmann, A., Natoli, G., and Ghosh, G. (2006). Transcriptional regulation via the NF-kappaB signaling module. Oncogene *25*, 6706–6716. https://doi.org/10.1038/sj.onc.120993350.

50. Pierce, J.W., Schoenleber, R., Jesmok, G., Best, J., Moore, S.A., Collins, T., and Gerritsen, M.E. (1997). Novel inhibitors of cytokine-induced IkappaBalpha phosphorylation and endothelial cell adhesion molecule expression show anti-inflammatory effects in vivo. J. Biol. Chem. *272*, 21096–21103. https://doi.org/10.1074/jbc.272.34.2109651.

51. Jimenez-Blasco, D., Santofimia-Castaño, P., González, A., Almeida, A., and Bolaños, J.P. (2015). Astrocyte NMDA receptors' activity sustains neuronal survival through a Cdk5-Nrf2 pathway. Cell Death Differ. *22*, 1877–1889. https://doi.org/10.1038/cdd.2015.4952.

52. Tonelli, C., Chio, I.I.C., and Tuveson, D.A. (2018). Transcriptional regulation by Nrf2. Antioxidants Redox Signal. *29*, 1727–1745. https://doi.org/10.1089/ars.2017.734253.

53. Kim, E.H., Sohn, S., Kwon, H.J., Kim, S.U., Kim, M.J., Lee, S.J., and Choi, K.S. (2007). Sodium selenite induces superoxide-mediated mitochondrial damage and subsequent autophagic cell death in malignant glioma cells. Cancer Res. *67*, 6314–6324. https://doi.org/10.1158/0008-5472.Can-06-4217.

54. Hackenberg, T., Juul, T., Auzina, A., Gwizdz, S., Malolepszy, A., Van Der Kelen, K., Dam, S., Bressendorff, S., Lorentzen, A., Roepstorff, P., et al. (2013). Catalase and no catalase activity promote autophagy-dependent cell death in Arabidopsis. Plant Cell *25*, 4616–4626. https://doi.org/10.1105/tpc.113.11719255.

55. Hensley, K., and Harris-White, M.E. (2015). Redox regulation of autophagy in healthy brain and neurodegeneration. Neurobiol. Dis. *84*, 50–59. https://doi.org/10.1016/j.nbd.2015.03.002.

56. Sheen, J.H., Zoncu, R., Kim, D., and Sabatini, D.M. (2011). Defective regulation of autophagy upon leucine deprivation reveals a targetable liability of human melanoma cells in vitro and in vivo. Cancer Cell *19*, 613–628. https://doi.org/10.1016/j.ccr.2011.03.012.

57. Xie, X., White, E.P., and Mehnert, J.M. (2013). Coordinate autophagy and mTOR pathway inhibition enhances cell death in melanoma. PLoS One *8*, e55096. https://doi.org/10.1371/journal.pone.005509658.

58. Soengas, M.S., and Lowe, S.W. (2003). Apoptosis and melanoma chemoresistance. Oncogene *22*, 3138–3151. https://doi.org/10.1038/sj.onc.1206454.

59. Komatsu, M., Waguri, S., Chiba, T., Murata, S., Iwata, J.i., Tanida, I., Ueno, T., Koike, M., Uchiyama, Y., Kominami, E., and Tanaka, K. (2006). Loss of autophagy in the central nervous system causes neurodegeneration in mice. Nature *441*, 880–884. https://doi.org/10.1038/nature0472360.

60. Hara, T., Nakamura, K., Matsui, M., Yamamoto, A., Nakahara, Y., Suzuki-Migishima, R., Yokoyama, M., Mishima, K., Saito, I., Okano, H., and Mizushima, N. (2006). Suppression of basal autophagy in neural cells causes neurodegenerative disease in mice. Nature *441*, 885–889. https://doi.org/10.1038/nature0472461.

61. Liang, C.C., Wang, C., Peng, X., Gan, B., and Guan, J.L. (2010). Neural-specific deletion of FIP200 leads to cerebellar degeneration caused by increased neuronal death and axon degeneration. J. Biol. Chem. *285*, 3499–3509. https://doi.org/10.1074/jbc.M109.072389.

62. Kuma, A., Hatano, M., Matsui, M., Yamamoto, A., Nakaya, H., Yoshimori, T., Ohsumi, Y., Tokuhisa, T., and Mizushima, N. (2004). The role of autophagy during the early neonatal starvation period. Nature *432*, 1032–1036. https://doi.org/10.1038/nature03029.

63. Wang, C., Liang, C.C., Bian, Z.C., Zhu, Y., and Guan, J.L. (2013). FIP200 is required for maintenance and differentiation of postnatal neural stem cells. Nat. Neurosci. *16*, 532–542. https://doi.org/10.1038/nn.336564.

64. Tang, G., Gudsnuk, K., Kuo, S.-H., Cotrina, M.L., Rosoklija, G., Sosunov, A., Sonders, M.S., Kanter, E., Castagna, C., Yamamoto, A., et al. (2014). Loss of mTOR-dependent macroautophagy causes autistic-like synaptic pruning deficits. Neuron *83*, 1131–1143. https://doi.org/10.1016/j.neuron.2014.07.040.

65. Boecker, C.A., and Holzbaur, E.L. (2019). Vesicular degradation pathways in neurons: at the crossroads of autophagy and endo-lysosomal degradation. Curr. Opin. Neurobiol. *57*, 94–101. https://doi.org/10.1016/j.conb.2019.01.005.

66. Hwang, J.-Y., Yan, J., and Zukin, R.S. (2019). Autophagy and synaptic plasticity: epigenetic regulation. Curr. Opin. Neurobiol. *59*, 207–212. https://doi.org/10.1016/j.conb.2019.09.01067.

67. Yamamoto, A., and Yue, Z. (2014). Autophagy and its normal and pathogenic states in the brain. Annu. Rev. Neurosci. *37*, 55–78. https://doi.org/10.1146/annurev-neuro-071013-014149.

68. Guo, F., Liu, X., Cai, H., and Le, W. (2018). Autophagy in neurodegenerative diseases: pathogenesis and therapy. Brain Pathol. *28*, 3–13. https://doi.org/10.1111/bpa.1254569.

69. Bubici, C., Papa, S., Dean, K., and Franzoso, G. (2006). Mutual cross-talk between reactive oxygen species and nuclear factor-kappa B: molecular basis and biological significance. Oncogene *25*, 6731–6748. https://doi.org/10.1038/sj.onc.1209936.

70. Jones, W.K., Brown, M., Ren, X., He, S., and McGuinness, M. (2003). NF-kappaB as an integrator of diverse signlaing pathways: the haer of myocardial signaling? Cardiovasc. Toxicol. *3*, 229–254. https://doi.org/10.1385/ct:3:3:22971.

71. Naito, Y., Yamada, T., Matsumiya, T., Ui-Tei, K., Saigo, K., and Morishita, S. (2005). dsCheck: highly sensitive off-target search software for double-stranded RNA-mediated RNA interference. Nucleic Acids Res. *33*, 589–591. https://doi.org/10.1093/nar/gki41972.

72. Owusu-Ansah, E., Yavari, A., and Banerjee, U. (2008). A protocol for *in vivo* detection of reactive oxygen species. Protoc. Exch. https://doi.org/10.1038/nprot.2008.23.

73. Wolff, T. (2011). Preparation of Drosophila eye specimens for transmission electron microscopy. Cold Spring Harb. Protoc. *2011*, 1386–1388. https://doi.org/10.1101/pdb.prot066514.

STAR★METHODS

KEY RESOURCES TABLE

REAGENT or RESOURCE	SOURCE	IDENTIFIER
Antibodies		
ARMS (rabbit polyclonal)	Liao et al. 2007[13] https://doi.org/10.1158/0008-5472.CAN-07-1930.	Huang's Lab (National Taiwan University Dept of Pathology, Taiwan)
LC3B (rabbit polyclonal)	Novus	Cat# NB100-2220; RRID:AB_10003146
ATG5 (rabbit polyclonal)	Novus	Cat# NB110-53818; RRID:AB_828587
Poly (ADP-ribose) polymerase (rabbit polyclonal)	Cell Signaling	Cat# 9542; RRID:AB_2160739
phospho-RelA/p65-Ser529 (rabbit polyclonal)	Santa Cruz	Cat# sc101751; RRID:AB_1128538
RelA/p65 (rabbit polyclonal)	Santa Cruz	Cat# sc-372; RRID:AB_632037
Catalase (goat polyclonal)	Santa Cruz	Cat# sc-34285; RRID:AB_2071744
SOD1(rabbit polyclonal)	Santa Cruz	Cat# sc-11407; RRID:AB_2193779
α-Tubulin (mouse monoclonal)	Santa Cruz	Cat# sc-5286; RRID:AB_628411
Cathepsin D (mouse monoclonal)	Abcam	Cat# ab6313; RRID:AB_305416
cleaved-Caspase 3 (rabbit polyclonal)	Abcam	Cat# ab49822; RRID:AB_868673
Nrf2 (goat polyclonal)	R&D Systems	Cat# AF3925; RRID:AB_11128044
HA (mouse monoclonal)	Sigma	Cat# H3663; RRID:AB_262051
MYC (mouse monoclonal)	Invitrogen	Cat# 13-2500; RRID:AB_2533008
Beclin 1 (rabbit polyclonal)	Abcam	Cat# ab62557; RRID:AB_955699
HRP-conjugated goat anti-mouse IgG	Abcam	Cat# ab205719; RRID:AB_2755049
HRP-conjugated goat anti-rabbit IgG	Abcam	Cat# ab205718; RRID:AB_2819160
Alexa Fluor 488 (or 594)-conjugated secondary antibodies (goat or donkey polyclonal)	Invitrogen	Cat# A32723; RRID:AB_2633275 Cat# A32731; RRID:AB_2633280 Cat# A32740; RRID:AB_2762824 Cat# A32744; RRID:AB_2762826
Bacterial and virus strains		
Lentivirus harboring pLKO.1-shAtg5	RNA technology Platform and Gene Manipulation Core, Academia Sinica, Taipei, Taiwan	Clone ID: TRCN0000099432
Chemicals, peptides, and recombinant proteins		
Hydrogen peroxide (H_2O_2)	Sigma-Aldrich	Cat# H1009
Bafilomycin A1	Sigma-Aldrich	Cat# B1793
Rapamycin	Sigma-Aldrich	Cat# R0395
Tiron	Sigma-Aldrich	Cat# D7389
N-acetyl-L-cysteine (NAC)	Sigma-Aldrich	Cat# A8199
Catalase-PEG	Sigma-Aldrich	Cat# C4963
Paraformaldehyde	Sigma-Aldrich	Cat# P6148
Triton X-100	Sigma-Aldrich	Cat# T8532
Boc-aspartyl-(OMe)-fluoromethyl-ketone (BAF)	Merck	Cat# B2682
H33258	Abcam	Cat# ab228550
3-(4, 5-dimethylthiazolyl-2)-2, 5-diphenyltetrazolium bromide (MTT)	Sigma-Aldrich	Cat# M5655
Dulbecco's modified Eagle's medium (DMEM)	Invitrogen™	Cat# 12100-046
Fetal bovine serum	ThermoFisher/Gibco™	Cat# 10099141

(*Continued on next page*)

Continued

REAGENT or RESOURCE	SOURCE	IDENTIFIER
L-Glutamine	Sigma-Aldrich	Cat# G7513
Penicillin-Streptomycin (10,000 U/mL)	ThermoFisher/Gibco™	Cat# 15140122
Lipofectamine™ 2000 transfection reagent	Invitrogen™	Cat# 11668019
Puromycin dihydrochloride	Sigma-Aldrich	Cat# P8833
5-(and-6)-chloromethyl-2′,7′-dichlorodihydrofluorescein diacetate, acetyl ester (CM-H_2DCFDA)	Invitrogen™	Cat# C6827
LysoTracker Red DND-99	Invitrogen	Cat# L7528
Protease inhibitor cocktail	ThermoFisher	Cat# 87786
Western Lightning® ECL Pro	PerkinElmer	Cat# NEL122001EA
Bradford Reagent	Merck	Cat# B6919
2.5% Glutaraldehyde in 0.1M Cacodylate Buffer	Electron Microscopy Sciences	Cat# 16537-15
Osmium Tetroxide	Electron Microscopy Sciences	Cat# 19152
Trichlorofluoromethane	Merck	Cat# 48541
Critical commercial assays		
Dual-Luciferase Reporter Assay System	Promega	Cat# E1910
Beta-Glo Assay System (Luminescent β-galactosidase Detection Kit)	Promega	Cat# E4720
Annexin V conjugates for apoptosis detection	ThermoFisher	Cat# A13201
Experimental models: Cell lines		
Mouse B16-F0 melanoma cell line	the American Type Tissue Culture Collection (ATCC)	CRL-6322; RRID:CVCL_0604
si*ARMS* melanoma cell line	Liao et al. 2007.	Huang's Lab (National Taiwan University Dept of Pathology, Taiwan)
si*Scramble* melanoma cell line	Liao et al. 2007[13] https://doi.org/10.1158/0008-5472.CAN-07-1930.	Huang's Lab
293FT	ThermoFisher Scientific/Invitrogen™	R70007
Experimental models: Organisms/strains		
Drosophila melanogaster *UAS-dARMS-dsRNA#1*	the Vienna *Drosophila* RNAi Center (VDRC, Vienna, Austria)	VDRC41732
UAS-dARMS-dsRNA#2	VDRC	VDRC45464
UAS-dorsal-dsRNA	VDRC	VDRC45998
GMR-GAL4/CyO	Bloomington *Drosophila* Stock Center	#9146
UAS-Dicer	Bloomington *Drosophila* Stock Center	#60008
UAS-mRFP	Bloomington *Drosophila* Stock Center	#7118
w^1 *P{UAS-Catalase}2*	Bloomington *Drosophila* Stock Center	#24621
UAS-mCD8::GFP	the Bloomington *Drosophila* Stock Center	#60698
UAS-Syt::GFP	Bloomington *Drosophila* Stock Center	#6925
UAS-Syb::GFP	Bloomington *Drosophila* Stock Center	#9263
UAS-IKKβ^{EY02434}	Bloomington *Drosophila* Stock Center	#60698
UAS-dARMS/TM6B	Dr. Y. Henry Sun	Sun's Lab (Institute of Molecular Biology, Academia Sinica, Taipei Taiwan)

(*Continued on next page*)

Continued

REAGENT or RESOURCE	SOURCE	IDENTIFIER
Oligonucleotides		
5′-GTGCCTACATAAATATC-3′	This paper	*dARMS*-F primer for RT-PCR, Huang's Lab
5′-CCAATATGGTCTTCTG-3′	This paper	*dARMS*-R primer for RT-PCR
5′-TACAGGCCCAAGATCGTGAA-3′	This paper	*Rp49*-F primer for RT-PCR internal control
5′-ACGTTGTGCACCAGGAACTT-3′	This paper	*Rp49*-R primer for RT-PCR internal control
5′-AACCAGTTGTGTTGTCAGGAC-3′	This paper	*Sod1*-F primer for Q-PCR
5′-CCACCATGTTTCTTAGAGTGAGG-3′	This paper	*Sod1*-R primer for Q-PCR
5′-AATCCTACACCATGTCGGACA-3′	This paper	*Catalase*-F primer for Q-PCR
5′-CGGTCTTGTAATGGAACTTGC-3′	This paper	*Catalase*-R primer for Q-PCR
5′-CTGAACTCCTGGACGGGACTA-3′	This paper	*Nrf2*-F primer for Q-PCR
5′-CGGTGGGTCTCCGTAAATGG-3′	This paper	*Nrf2*-R primer for Q-PCR
5′-AGGATGGGAGGTACTCGAATC-3′	This paper	*Nqo1*-F primer for Q-PCR
5′-TGCTAGAGATGACTCGGAAGG-3′	This paper	*Nqo1*-R primer for Q-PCR
5′-TATACTAGTGCTGGTCTTGGATTTTGTCAC-3′	This paper	*Txnrd1*-F primer for Q-PCR
5′- ATAGAATTCCAAGGCGACATAGGATGCAC-3′	This paper	*Txnrd1*-R primer for Q-PCR
5′- TGTTACCAACTGGGACA-3′	This paper	*Actin*-F primer for Q-PCR control
5′-GGGGTGTTGAAGGTCTCAAA-3′	This paper	*Actin*-R primer for Q-PCR control
Recombinant DNA		
pARMS-MYC	Liao et al. 2007[13] https://doi.org/10.1158/0008-5472.CAN-07-1930.	Huang's Lab
pGFP-LC3 plasmid	Dr. Ann-Lii Cheng	Cheng's Lab (National Taiwan University Cancer Center, Taipei, Taiwan)
pHA-IKKβ-SS/EE plasmid pHA-IKKβ-SS/AA plasmid pHA-IKKβ-WT plasmid	Dr. Li-Chung Hsu	Hsu's Lab (National Taiwan University College of Medicine Institute of Molecular Medicine, Taiwan)
pGL3-basic Luciferase reporter vector	Promega	Cat# E1751
Software and algorithms		
GraphPad Prism version 9	GraphPad Software Inc., USA	GP9-1948506-RKRC-BD42A
SigmaPlot 14	StarCom Information Technology	Serial No: 775460200
MetaMorph image analysis software, version 7.6.4.0	Molecular Devices	System ID:33296

RESOURCE AVAILABILITY

Lead contact

Requests for further information regarding reagents and resources used in this study should be directed to lead contact, Dr. Pei-Hsin Huang (phhuang@ntu.edu.tw).

Materials availability

This study did not generate new unique reagents. Plasmids, si*ARMS* melanoma cell lines, and *UAS-dARMS/TM6B drosophila* strain generated in this study are available upon request from the lead contact with a completed Material Transfer Agreement.

Data and code availability

This paper did not generate original code. Any additional information required to reanalyze the data reported in this paper is available from the lead contact upon request.

EXPERIMENTAL MODEL AND SUBJECT DETAILS

Cell culture, transfection, drug treatment, and virus transduction

Mouse B16-F0 melanoma cell line was maintained in Dulbecco's modified Eagle's medium supplemented with 10% fetal bovine serum, 2 mM L-glutamine, 100 μg/ml streptomycin, and 100 U/ml penicillin. B16-F0 with *ARMS*-knockdown stable cell lines (si*ARMS*) were established by RNAi approach and maintained as previously described.[13] Lipofectamine 2000 was used for transient transfection as manufacturer instructed. To generate recombinant lentivirus carrying *ATG5*-specific or scrambled small interfering RNA, 293FT cells were co-transfected with the package, envelope, and shRNA-expressing constructs. The virus-containing supernatant was then harvested and used to infect cells, which were selected and maintained with 2 μg/ml puromycin.

For various drug/chemical treatment, the *in vitro* cultured cells were pre-treated for 1 h with each indicated chemical including BAF (50 μM), Bafilomycin A1 (10 nM), rapamycin (50 nM), N-acetyl cysteine (NAC, 1 μM), tiron (2 μM), and PEG-catalase (1000 IU) followed by 50 μM H_2O_2 treatment for another 16 hr. The cells were then harvested and manipulated for other experiments.

Drosophila melanogaster stocks and genetics

Drosophila stocks were maintained on standard cornmeal agar media at 27°C unless otherwise noted. Eye phenotypes were examined and scored as described by Pandey et al..[40] The different *drosophila* strains used in this study were obtained either from the Vienna *Drosophila* RNAi Center or from the Bloomington *Drosophila* Stock Center as listed in the resources table. Note, the targeted sites for each *UAS-dARMS-dsRNA* line were as follows: *UAS-dARMS-dsRNA#1*, 1933-2301; *UAS-dARMS-dsRNA#2*, 4018-4303 (number indicates the distance from the start codon). All of the 19-mers in the targeting sequences were compared with the other targeting sequences using dsCheck.[71] The *GMR>UAS-hs-GFP-ATG8a,dARMS-dsRNA#1/+* fly was generated from our fly core laboratory. The *UAS-dARMS* transgene was generated by subcloning the 4120 bp SD10882 *dARMS* cDNA (BT009928) into the pUAST (w+) transformation vector. The construct was introduced into *w1118* embryos by P element-mediated transformation. The transformants were identified on the basis of eye pigmentation to establish several independent lines with insertions located on X, 2nd, and 3rd chromosomes. Several lines with insertions on the 2nd chromosome were crossed with flies carrying *dARMS-dsRNA#1* allele to obtain *GMR>dARMS^{RNAi}, dARMS* flies.

METHOD DETAILS

ROS detection and H_2O_2 treatment in fly

To detect the presence of ROS in different strains of fly, eye discs with mouth hooks of the 3rd instar larvae were carefully dissected (without severing) in 1X PBS, immediately incubated with 10 μM CM-H_2DCFDA in fresh Schneider's medium for 5 minutes in a dark chamber at room temperature, followed by three 5-minute washes in 1X PBS.[72] The samples were then mounted in Vectashield mounting media and imaged immediately using a confocal microscopy (Leica).

For H_2O_2 treatment in adult fly, we used filter paper soaked with 4% H_2O_2 dissolved in 5% sucrose solution in vials where 1-day-old flies were kept for 48 hours followed by preparation for scanning or transmission electron microscope.

MTT assay

Cultured cells treated with H_2O_2 or the buffer was changed to serum-free medium containing 5 mg/ml 3-(4, 5-dimethylthiazolyl-2)-2, 5-diphenyltetrazolium bromide (MTT) and incubated for another 4 h followed by adding an equal volume of isopropanol/0.04 M HCl. After centrifugation at 10,000 g for 5 min, the absorbance of the supernatant was measured at wavelength 570 nm and reference wavelength 630 nm with an enzyme-linked immunosorbent assay plate reader (ELX-800; Biotek).

Luciferase reporter assays

The si*Scramble*- and si*ARMS*- B16-F0 melanoma cells were transfected with the NF-κB luciferase reporter along with β-galactosidase DNA using lipofectamine 2000. Forty-eight hours after transient transfection, cells were left untreated or treated with 50 μM H_2O_2 for another 2 h. Cells were extracted by reporter lysis buffer using a Luciferase Reporter Assay System and luciferase activity was measured using a microplate

luminometer (Wallac Victor^{2TM}, PerkinElmer). The luciferase activity was assessed by normalization to the β-galactosidase activity.

Flow cytometry

Cells treated with 50 μM H_2O_2 for 16 h were collected, washed with ice-cold phosphate-buffered saline (PBS), and stained with Annexin V labeled by AlexaFluor 488 for assessing phosphatidyl-serine externalization by flow cytometry (BD FACSCalibur). The intracellular ROS level was detected by flow cytometry using 5-(and-6)-chloromethyl-2′,7′-dichlorodihydrofluorescein diacetate, acetyl ester (CM-H_2DCFDA). Cells were treated with 50 μM H_2O_2 for the indicated time, followed by staining with CM-H_2DCFDA (10 μM) in pre-warmed PBS for additional 15 min at 37 °C. After recovery in growth medium for 5 min, the cells were resuspended in PBS and were analyzed by flow cytometry (BD FACSCalibur).

Western blotting

Samples (cultured cells) were harvested and lysed in sampling buffer (150 mM NaCl, 50 mM Tris-HCl pH 7.4, 1% Nonidet P-40, 0.25% Na-deoxycholate, 1 mM EDTA, protease inhibitor cocktail, 1 mM phenylmethylsulfonyl fluoride, 1 mM NaF, and 1 mM Na_3VO_4). Protein concentration was measured using the Bradford reagent and around 30 μg of total proteins was subjected to SDS-PAGE followed by immunoblotting. An enhanced chemiluminescence reaction was applied for signal detection.

Antibodies were used in immunoblot as follows: LC3B (1:500), ATG5 (1:1000), poly(ADP-ribose) polymerase (1:1000), phospho-RelA/p65-Ser529 (1: 200), RelA/p65 (1:200 for immunoblot; 1:50 for immunofluorescence), Catalase (1:200 for immunoblot; 1:50 for immunofluorescence), SOD1 (1:200), α-Tubulin (1:1000), Cathepsin D (1:1000), cleaved-Caspase 3 (1:100), HA (1:10000), MYC (1:1000), Beclin 1 (1:1000), ARMS (1:1000), HRP-conjugated goat anti-mouse (1:500), anti-rabbit IgG (1:500), Alexa Fluor 488 (or 594)-conjugated secondary antibodies (1:1000) and H33258 (1:1000).

Immunofluorescence microscopy

B16-F0 cells were grown on coverslips at a density of 8 x 10^4 cells per well in a 12-well plate 1 day before transfection. Twenty-four hours after transfection, the cells were treated with or without H_2O_2 for 16 h, fixed with 4% paraformaldehyde, and permeabilized with 0.1% triton X-100. Cells were then processed for immunostaining and the fluorescent images were obtained by epifluorescence or confocal microscopy (Leica TSC SP5). Antibodies were used as follows: RelA/p65 (1:50), MYC (1:200), Catalase (1:50). Quantification of GFP-LC3 puncta was performed using MetaMorph image analysis software, version 7.6.4.0 (Molecular Devices). For LysoTracker Red co-stain, the cells were treated with 75 nM LysoTracker Red DND-99 for 60 min at 37 °C before harvesting, and washed three times in PBS followed by PFA fixation and imaging.

For fluorescence microscopy of *drosophila*, the eye discs of the wandering third instar larvae were dissected in PBS containing pin/cyo fly lysates, fixed in 4% paraformaldehyde for 30 min at room temperature, washed with PBS three times, and mounted in glycerol mounting medium. For ROS detection, the dissected eye discs were pre-stained in 10 μM CM-H_2DCFDA /PBS solution for 30 min at 37°C before fixation. The fluorescence was analyzed under a confocal microscopy (Leica).

Electron microscopy

Cells treated with/ without H_2O_2 (50 μM) for 16 h were harvested by trypsinization, washed with PBS, and fixed with 2.5% glutaraldehyde in 0.1 M cacodylate buffer for 30 min at room temperature. After washing with PBS, the samples were post-fixed in 1% osmium tetroxide. The samples were then processed to make ultrathin Epon-embedded sections for transmission electron microscopic observation (Hitachi H-7000). For morphologic analysis of autophagic vacuoles, at least 20 cells of each sample were analyzed.

For transmission electron microscopy examination of fly eyes, the protocol published by Wolff is followed.[73] Briefly, the larva or adult head were injected with fixative (0.1 M sodium cacodylate, pH 7.4, 4% formaldehyde, 3.5% glutaradldehyde), followed by overnight-fixation in 1% tannic acid. The sample then was washed with 0.1 M sodium cacodylate, infiltrated with 2% OsO4 for 2h, rinsed in water, and incubated in 2% uranyl acetate at room temperature overnight. The tissue was dehydrated through a graded ethanol and processed for embedding and microtome sectioning. For scanning electron microscopy (SEM), the head of adult flies were dissected, immersed through a series of graded ethanol (25%, 50%, 75%, 100%)

at room temperature for days, followed by a series of trichlorofluoroethane diluted in 100% ethanol (25%, 50%, 75%, 100% trichlorogluoroethane; each at room temperature for 12 h). The samples were then removed, dried under a vacuum, and mounted for SEM.

QUANTIFICATION AND STATISTICAL ANALYSIS

All data were analyzed and graph plotted by using PRISM GraphPad Software (La Jolla, CA, USA), are shown as mean ± SD. Statistical significance was determined either by Student's *t*-test, or Mann-Whitney rank sum test, or One Way ANOVA. A *P*-value < 0.05 was considered statistically significant.